



Contents lists available at ScienceDirect

Quaternary International

journal homepage: www.elsevier.com/locate/quaint

Tephrostratigraphy and petrological study of Chikurachki and Fuss volcanoes, western Paramushir Island, northern Kurile Islands: Evaluation of Holocene eruptive activity and temporal change of magma system

Takeshi Hasegawa^{a,*}, Mitsuhiro Nakagawa^b, Mitsuhiro Yoshimoto^b, Yoshihiro Ishizuka^c, Wataru Hirose^d, Sho-ichi Seki^e, Vera Ponomareva^f, Rybin Alexander^g

^a Department of Earth Sciences, College of Science, Ibaraki University, 2-1-1, Bunkyo, Mito 310-8512, Japan

^b Department of Natural History Sciences, Faculty of Science, Hokkaido University, N10 W8, Kita-ku, Sapporo 060-0810 Japan

^c Geological Survey of Japan, National Institute of Advanced Industrial Science and Technology (AIST), AIST Tsukuba Central 7, 1-1, Higashi 1-Chome, Tsukuba, Ibaraki 305-8567, Japan

^d Geological Survey of Hokkaido, N19 W12, Kita-ku, Sapporo 060-0819, Japan

^e Mitsubishi Material Corporation Higashitani Mine, 750 Komori, Kokuraminami-ku, Kitakyushu 803-0182, Japan

^f Institute of Volcanology and Seismology, 9 Piip Boulevard, Petropavlovsk-Kamchatsky 683006, Russia

^g Institute of Marine Geology and Geophysics, 5 Nauka Street, Yuzhno-Sakhalinsk 693022, Russia

ARTICLE INFO

Article history:

Available online 19 July 2011

ABSTRACT

A tephrostratigraphic and petrological study of the Chikurachki (1816 m)-Tatarinov-Lomonosov volcanic chain (CTL volcanic chain) and Fuss (1772 m), located at the southern part of Paramushir Island in the northern Kurile Islands, was carried out to reveal the explosive eruption history during the Holocene and the temporal change of the magma systems of these active volcanoes. Tephra successions were described at 54 sites, and more than 20 major eruptive units were identified, consisting of pumice fall, scoria fall and ash fall deposits, each of which are separated by paleosol or peat layers. The source volcano of each recognized tephra layer was confirmed by correlation with proximal deposits of each eruption center with respect to petrography and whole-rock and glass chemistry. The age of each layer was determined by radiocarbon dating and the stratigraphic relationship with the dated, widespread tephra from Kamchatka according to the thickness of paleosols bracketed between tephra layers. The Holocene activity in this region was initiated by eruptions from the Tatarinov and Lomonosov volcanoes. After the eruptions, the Fuss and Chikurachki volcanoes started their explosive activities at ca. 7.5 ka BP, soon after the deposition of widespread tephra from the Kurile Lake caldera in southern Kamchatka. Compared with Fuss located on the back-arc side, Chikurachki has frequent, repeated explosive and voluminous eruptions. Whole-rock compositions of the rocks of the CTL volcanic chain and Fuss are classified into medium-K and high-K groups, respectively. These suggest that magma systems beneath the CTL volcanic chain and Fuss differ from each other and have been independently constructed. The rocks of the Chikurachki volcano are basalt-basaltic andesite and have gradually evolved their chemical compositions; when graphed on a SiO₂-oxide diagram, these form smooth trends from mafic to more felsic. This suggests that the magma system evolved mainly by fractional crystallization. In contrast, matrix glass chemistries for Fuss pumices are distinct for each eruption and show different K₂O levels on a SiO₂-K₂O diagram. This implies that the magma system of Fuss has been frequently replaced. Both volcanoes have been active under the same subduction system. However, the Chikurachki volcano will continue eruptive activity under a stable magma system with a higher magma discharge rate, whereas Fuss may continue construction with an intermittent supply of distinct, small magma batches.

© 2011 Elsevier Ltd and INQUA. All rights reserved.

1. Introduction

Volcanoes in an arc-trench system usually form a volcanic cluster and/or chain (Tamura et al., 2002). Formation processes of

the cluster (or chain) and geochemical data on erupted magma are fundamental data needed to discuss the processes of subduction-related magmatism. The powerful tools of tephrochronology, combined with the geochemical fingerprinting of tephra layers, can construct the eruptive history of a volcanic region (e.g., Braitseva et al., 1995; Seymour et al., 2004; Kutterolf et al., 2007; Wulf et al., 2008). In addition, the geochemical and petrological data of

* Corresponding author.

E-mail address: hasegawt@mx.ibaraki.ac.jp (T. Hasegawa).

proximal deposits of each volcanic center in a volcanic region can be used to identify a tephra layer from each adjacent volcano (Bice, 1985; Kutterolf et al., 2007; Hasegawa et al., 2009). These studies could reveal the temporal and spatial evolution of the volcanic activity and magma system at each eruption center.

The Kurile Islands, the adjacent Kamchatka peninsula and Japanese Islands make up one of the earth's most active regions in which subduction-related phenomena occur, including earthquakes and volcanic eruptions. More than 48 Holocene volcanoes are situated in the Kurile Islands, 30 of which have erupted during historical time with several occurrences of explosive eruptions (more than VEI = 4) (Gorshkov, 1970; Siebert and Simkin, 2002). According to the core survey of marine sediments in Pacific Ocean, frequent explosive eruptions have continued in the region at least since the Pliocene (Cao et al., 1995; Prueher and Rea, 2001). However, the correlation of each ash layer in the cores with the source volcano and/or volcanic region in the islands has not been adequately clarified. Although the general geological structure and eruption history of each island has been already reviewed by Ostapenko et al. (1967) and Gorshkov (1970), systematic and extensive tephrostratigraphy and tephrochronology remain unclear except for the studies focusing on recent explosive eruptions of extremely active volcanoes (Tyatya volcano (Fig. 1); Nakagawa et al., 2002; Chikurachki volcano: Belousov et al., 2003).

This paper presents the Holocene tephrostratigraphy for the southwestern part of Paramushir Island in the northern Kurile Islands, where the Chikurachki, Fuss and several other active volcanoes have exhibited repeated explosive eruptions and lava effusion. In addition to field observations and the petrographical description of each tephra layer, geochemical analyses of rock samples and AMS radiocarbon analysis were performed to examine the frequency of explosive eruptions and the evolution of magma

systems at each volcanic center. Investigations revealed the systematic temporal and spatial changes of the modes, scales and frequencies of eruptions of each active volcano, in addition to the temporal evolution of the magma systems.

2. General geology

Four active volcanoes, Chikurachki, Tatarinov, Lomonosov and Fuss, are located on the southern part of Paramushir Island in the northern Kurile Islands, where the westward subduction of the Pacific plate under the North American Plate occurs. The former three volcanoes form an NNE–SSW trending volcanic chain, (Chikurachki-Tatarinov-Lomonosov (CTL) volcanic chain) at the north end of the Karpinsky Ridge (Fig. 1, Fig. 2a). Fuss is a unique, isolated peak, forming a distinct peninsula near the southwest coast of the island (Fig. 2b). Neogene basement rocks, primarily composed of volcanic rocks, are widely distributed on the southern and eastern side of the volcanic area (Nemoto and Sasa, 1960). Holocene eruptive deposits from these volcanoes cover the Pleistocene volcanic rocks that are exposed at the foot of these volcanoes (Fig. 3).

The Chikurachki volcano (1816 m) is the highest volcano on Paramushir Island and the third highest in the Kurile Islands. The volcano is a quite active, basaltic-andesitic stratovolcano that has exhibited explosive eruptions more than 10 times since 1853 (Belousov et al., 2003; Gurenko et al., 2005; Girina et al., 2008). These historical eruptions comprise two dominant eruptive styles: plinian (1853 and 1986) and strombolian (others) (Ovsyannikov and Muraviev, 1992; Belousov et al., 2003). The Tatarinov and Lomonosov volcanoes, adjoining Chikurachki on the south, are also stratovolcanoes with summit craters and lava domes (Fig. 3). These edifices are slightly eroded compared with that of Chikurachki,

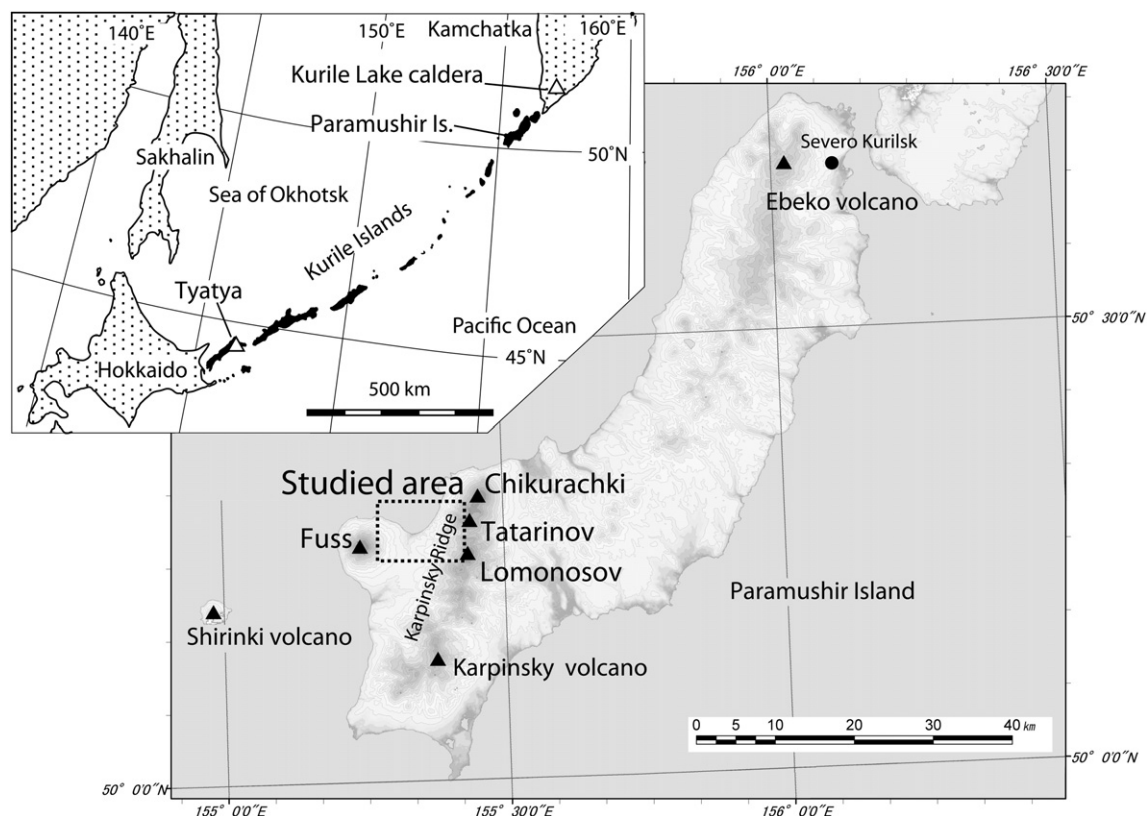


Fig. 1. Index map showing the location of Paramushir Island, the distribution of Holocene volcanoes and the studied area.

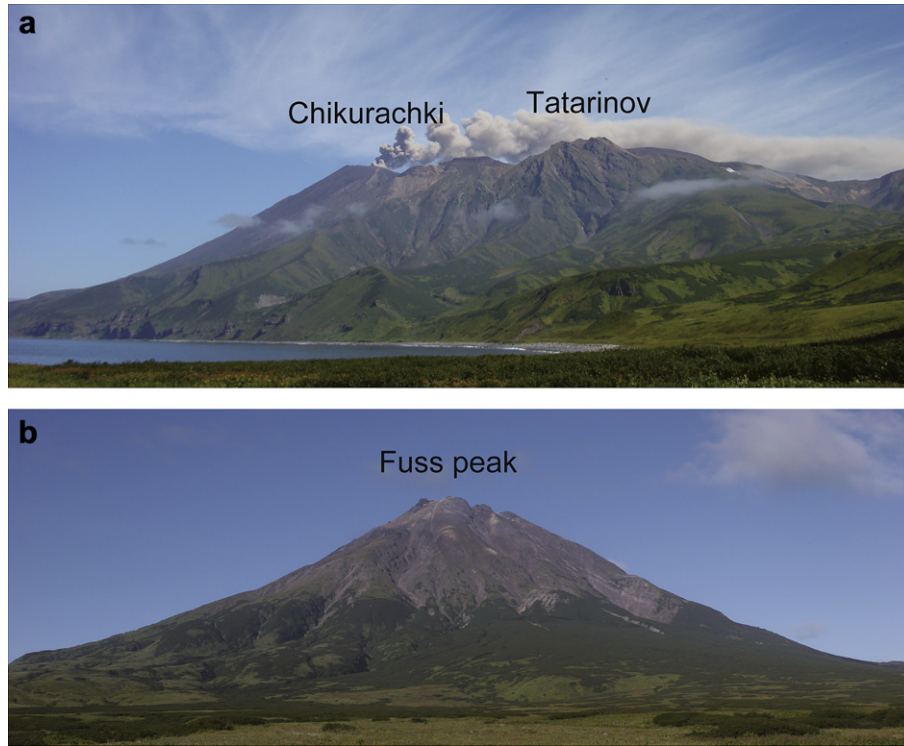


Fig. 2. Photographs of the Chikurachki and Fuss volcanoes from the base camp (BC), the location of which is shown in Fig. 3. (a) Easterly view of the erupting Chikurachki volcano taken on 8 September 2007. The Tatarinov volcano is the highest peak of this photograph, 3 km south (right) from Chikurachki. (b) Westerly view of Fuss.

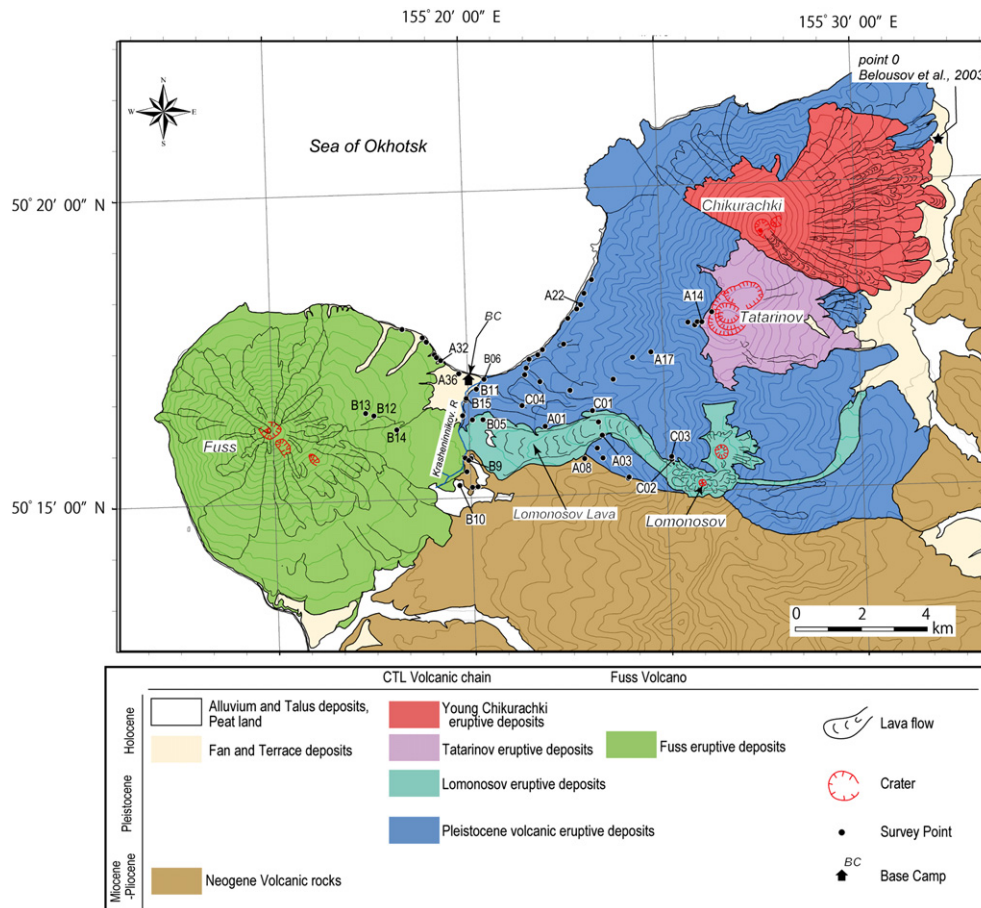


Fig. 3. Simplified geologic map of the studied area (based on Nemoto and Sasa, 1960 and satellite images) with survey points. The number of representative outcrops for description and sampling are also shown. In addition, Section 0 described by Belousov et al. (2003) is shown (see Fig. 15). The contour interval is 100 m.

suggesting their ages date from the latest Pleistocene to the Holocene. Lava flow from Lomonosov preserves its primary surface morphology and extends more than 7 km westward from the crater reaching the main river (Krashennnikov River; Fig. 3). This lava flow has been described by Gorshkov (1970) as a Holocene eruptive product.

The Fuss peak (1772 m) is located about 17 km west at the back-arc side of the CTL volcanic chain (Fig. 3). The volcano is an andesitic-dacitic stratovolcano with numerous well-preserved lava flows and summit craters. A high content of hornblende phenocryst characterizes the rocks from the volcano, a feature uncommon to the rocks of the CTL volcanic chain (Gorshkov, 1970). Only one authentic (and strongly explosive) historical eruption took place in 1854 (Gorshkov, 1970).

3. Techniques and conventions

3.1. Field procedures

A geological survey was performed for 12 days over an area of 80 km² (Fig. 1), including both the western part of the CTL volcanic chain and the eastern foot of Fuss (Fig. 3). Numerous stratified tephra layers overlie the thick lahars and debris avalanche deposits that lie at the base of sections along the Krashennnikov River (Figs. 4c and 5). The Lomonosov lava is interbedded with these tephra layers. The tephra succession, particularly the stratigraphic relationships and tephra dispersals, was described at 54 outcrops in this area. As a result, more than 40 units of volcanoclastic deposits including pumice fall, scoria fall and ash fall deposits and products of small phreatic eruption with accretionary lapilli and reworked deposits were identified. These units vary in size, from a few centimeters to several meters in thickness. The focus was on 27 units that are widely distributed in the studied area. The following parameters were measured for each eruptive unit: total thickness, average diameter of the three largest clasts and grain size for ash layers (grain-size divisions are those of Wentworth, 1922). Interbedded paleosol or peat layers represent significant dormancy periods.

Tephra correlations are based on lithofacies (e.g., types of juvenile materials, sedimentary structures), stratigraphic positions and thickness, modal and chemical compositions of juvenile materials and radiocarbon dates. To determine the source volcanoes of these tephra layers, the correlations between the distal tephra layers and proximal deposits (tephra and lava) from each volcano were investigated on the basis of petrological features, such as mineral assemblage and whole-rock and matrix glass chemistry. Minimum approximate volumes of air-fall deposits were estimated from the single isopach using the method of Legros (2000). Volumes of lava and pyroclastic flow deposits were also calculated from their estimated minimum distribution areas and average thicknesses.

3.2. Laboratory procedures

Microscopic observations and modal analyses (approximately 2000 points on a thin section) of juvenile materials in each unit were completed. Glass compositions of selected thin sections were determined by the SEM-EDS system (JEOL JSM-T330A + LINK ISIS). Operating parameters were set at 15 kV for the accelerating voltage with beam diameter of 5 µm and count rate of 2.0 kcps for 180 s. Some scoria samples with microlite-rich matrix were analyzed by broad 10–50 µm beam. Corrections of the analyses were made according to the ZAF method. Five to ten glass composition analyses per sample were performed. Whole-rock compositions of major and trace elements were determined by X-ray fluorescence (XRF), using PANalytical Magix Pro. Washed and dried rock samples were

powdered using an agate mill. In the case of units containing small-sized pumice or scoria, several clasts (>1 cm in diameter) were combined to make rock powder for a glass bead. A XRF analysis of the fine-grained layer (<1 cm in diameter) was not performed. In the following part, water-free and normalized major element chemistry of glass shards and whole-rock was used.

New radiocarbon dating using accelerator mass spectrometry (AMS) was performed at the Institute of Accelerator Analysis Ltd, Japan. Seven peat and brown soil samples below or above volcanoclastic products were processed. The resulting radiocarbon ages (BP) were also calibrated into calendar years before present (cal BP) using the Calib 5.0 program (Stuiver et al., 2005). The calibrated ages are shown in Table 4.

4. Tephrostratigraphy

4.1. Descriptions of each layer

On the basis of lithofacies and petrographic features, the observed tephra units can be divided into four series in the field as follows: Olivine-pyroxene scoria (OSC), Hornblende pumice (HPM), Pyroxene pumice (PPM), and distal fine ash layers. Eleven OSC layers (OSC1–11, in descending order), eight HPM layers (HPM1–8), three PPM layers (PPM1–3), and two distal ash layers (yellowish ash, YA, and greenish ash, GA) were identified. These tephra are all air-fall deposits except for PPM1. The PPM layers were recognized beneath the Lomonosov lava, whereas the OSC and HPM ones are commonly located above the lava flow. In general, the lower part of the outcrops is rich in HPM layers, whereas OSC layers gradually dominate towards the top (Fig. 5). The detailed facies of each layer are described below.

4.1.1. Tephra layers

4.1.1.1. Olivine-pyroxene scoria layers (OSC layers). Observed at the sections close to Chikurachki, olivine-pyroxene scoria layers (OSC1–11) are blackish, well-sorted and mantle-bedding pyroclastic fall deposits composed of clast-supported scoriae. Juvenile materials (scoria) are poorly vesiculated, angular to sub-rounded in shape and characterized by the presence of olivine and clinopyroxene phenocrysts. The maximum grain size and total thickness of the OSCs increases towards Chikurachki. Very thin (<1 or 2 centimeters thick), poorly continuous scoria fall layers showing the same lithological feature as OSCs were also frequently recognized at the site closer to Chikurachki.

At Section C04, located approximately 9 km southwest of the Chikurachki summit crater, successive scoria fall layers of OSC1–5 separated by very thin soil layers were preserved between hornblende pumice layers (HPM1 and 2, described below) in the upper part of the section (Figs. 4 and 5). Their thicknesses are 2–6 cm and the sizes of the scoria lapilli are as large as 10 mm (Table 1). OSC3 is the largest in thickness and grain size. At several sections farther than C04 from the summit of Chikurachki (e.g., B15), each scoria layer of OSC1–5 between HPM1 and 2 could not be defined and were observed as a single scoria layer showing various vertical gradings of grain-size. OSC6–10 are located between the HPM2 and 4 at Sections A08, C04, B15 and B10. Thin (<1 or 2 cm) paleosol layers also intercalated with each fall deposit. Among them, OSC6 can be observed between HPM4 and 3 at B15. The scoria layers observed at A08, one of the sections nearest to the Chikurachki summit, are clearly thicker than those at the other localities. The thicknesses and maximum grain sizes of each layer of OSC6–10 are up to 4 cm and 2 mm at A08, respectively. Scoria fall deposits of OSC11 were widely observed below HPM8 (e.g., A08, C04 and B15). The thickness of the layer is 10 cm, and the maximum grain size is over 10 mm at Section A08. At the flank of Fuss (e.g., Section B14),



Fig. 4. Photographs of key sections. The locations of the sections are shown in Fig. 3. (a) Each of OSC1–5, OSC6–10 and numerous scoria layers can be recognized at C04. The scale is 80 cm long. (b) A08 section exposing from HPM6 to uppermost HPM2. The scale is 2 m long. (c) Pile of tephra layers overlying a thick volcanic lahar deposit with a man for scale at B14. (d) YA and GA below the HPM6. Many locally recognized phreatic eruption and cross-laminated reworked deposits can be found at the B15. The scale is 1 m.

the OSC layers are very well sorted and more finely grained. Some of the OSC6–10 layers cannot be observed here.

4.1.1.2. Hornblende pumice layers (HPM layers). Eight, white to yellowish white-colored pumiceous layers (HPM1–8) were found at the sections along the Krashennikov River and at the flank of Fuss. Their maximum grain size, thickness and number of layers increase towards Fuss (Fig. 5). Several layers of these, such as HPM1, 2, 5 and 6, are widely distributed in this area with eastward dispersal axes. These juvenile pumices are characterized by the presence of hornblende phenocrysts with small amounts of pyroxene phenocrysts.

HPM1, the uppermost major tephra unit in this area, was generally observed 10–15 cm beneath the surface. The tephra is

widely distributed and was also found at the slope of Chikurachki. HPM1 is preserved as a well-sorted and normal-grading pumice fall layer at section A32 and A36 along the east cost of Fuss. However, at other sections, the layer often consists of a poor-sorted mixture of white and banded pumice, lithic fragments and adhering fine ash. HPM4 is also a poor-to-well-sorted pyroclastic deposit composed of cohesive ash, white-colored pumice lapilli and lithic fragments. The maximum grain size of this layer is larger than those of the other HPM layers (80 mm at B15 and 40 mm at A08). These moderately sorted HPM4 and HPM1 layers are not considered to be pyroclastic flow deposits but as a coeval deposit of phreatoplinian ash and pumice fall (e.g., Smith and Houghton, 1995), judging from the cohesive matrix with angular pumices and uniform thicknesses in each observed section.

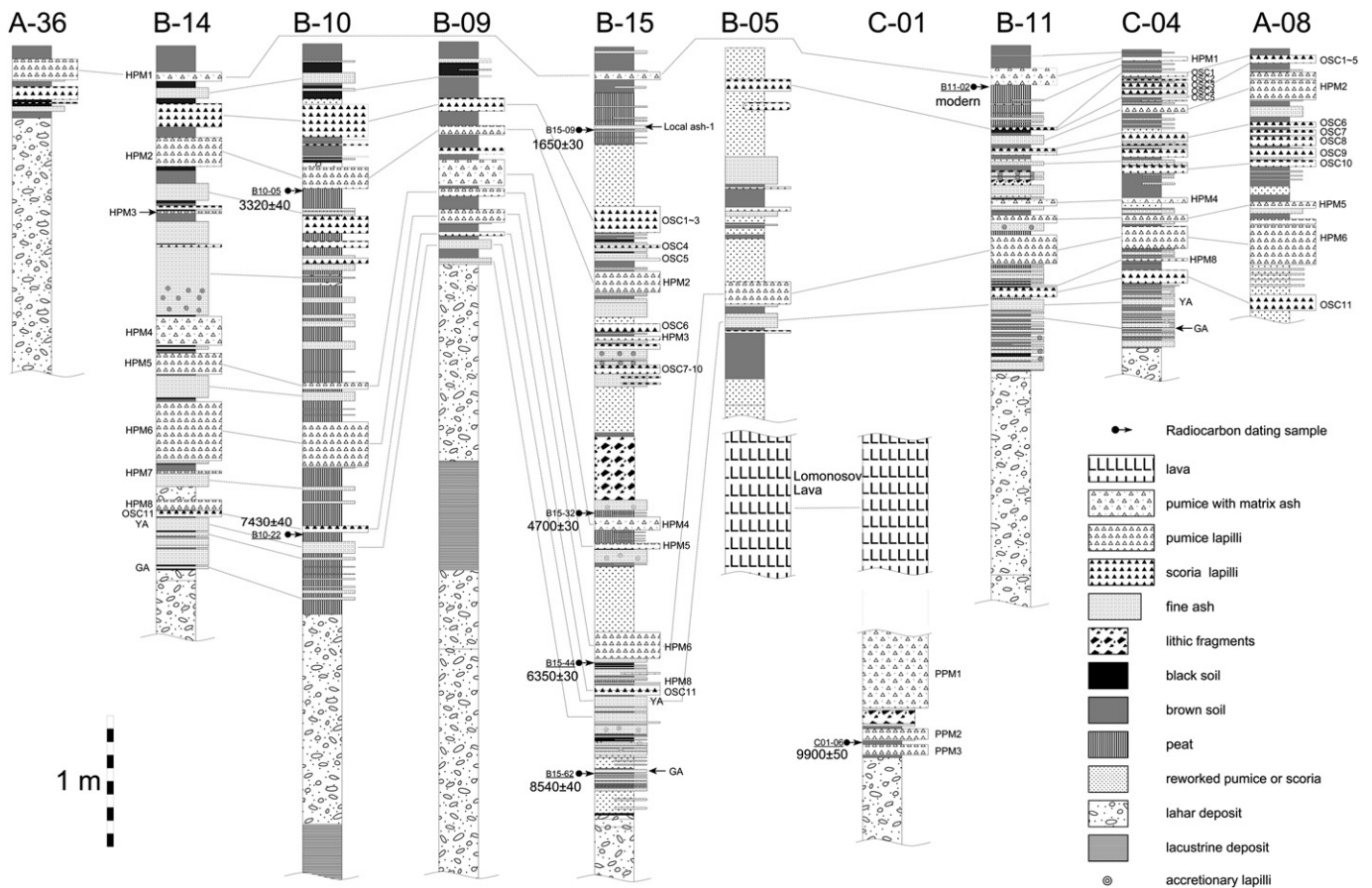


Fig. 5. Columnar sections between the Chikurachki and Fuss volcanoes. The localities of the sections are shown in Fig. 3. Arrows indicate the radiocarbon date of soil or peat layers.

HPM6 consists of a thick pumice fall deposit accompanied with a thin gray ash layer at the bottom. The thickness and maximum grain size of the fall deposit are approximately 40 cm and up to 20 mm at Section B15, respectively. The gray ash layer is approximately 1 cm thick. Although the deposit predominantly consists of white pumice, approximately 10 vol.% of banded and gray pumices appeared. HPM6 can be easily identified in the field due to its characteristic facies (gray ash, banded pumice and large-thickness), and it is useful as a key bed in this area. At Section B15, HPM2 and HPM5 contain white and gray pumice and are 16 cm and 4 cm thick with maximum grain sizes of 20 mm and 10 mm, respectively. The relatively small-scale pumice fall deposits, HPM3, 7 and 8, were observed only on the slope of Fuss. At Section B14, their thicknesses are 2–8 cm and maximum grain size are up to 20 mm. Fig. 6 displays the lateral variation of thicknesses for HPM1, 2, 4, 5 and 6.

4.1.1.3. Pyroxene pumice layers (PPM layers). Clinopyroxene-Orthopyroxene pumice deposits (PPM1–3) were observed below the Lomonosov lava at Section C01 about 7 km southwest of Chikurachki. They consist of two well-sorted pumice fall deposits (PPM2 and 3) with overlying pyroclastic flow deposits (PPM1) (Figs. 5, 7). Between these three layers, thin (2–5 cm thick) paleosols were recognized. PPM1 is structureless, brownish white, composed of pumice clasts and a fine-to-medium sand-sized ash matrix. The thickness is more than 60 cm, and the upper third is weakly oxidized. The maximum grain size of the white pumice (the main juvenile material) is approximately 3 cm. In addition to the white pumice, gray pumice and lithic fragments of altered rocks were also included. A yellowish-brown colored lithic layer, sandwiched by grayish, thin (1–2 cm thick) ashes, was recognized

directly beneath PPM1. PPM2 and 3 are located under PPM1, interbedded by paleosol layers. PPM2 and 3 are composed of angular to sub-rounded pumice clasts and with 10–20% of each being lithic fragments. The thicknesses of these two layers are both approximately 8 cm. The maximum sizes of the pumice clasts are 2 and 2.5 cm, respectively, and layers of lithic fragments are approximately 1.5 cm in diameter. At the base of PPM2, a grayish fine ash layer (1 cm in thickness) was observed. Pumices in PPM1 and 3 are white and well vesiculated. The juvenile materials of these PPM layers contain clinopyroxene and orthopyroxene phenocrysts without hornblende phenocrysts. PPM2 contains moderately vesiculated pumice that contains clinopyroxene and orthopyroxene phenocrysts with a minor amount of olivine.

4.1.1.4. Distal ash layers. Two structureless ash layers (YA and GA) displaying characteristic colors were found at some localities (Figs. 4 and 5). YA is a very well-sorted (very fine sand to medium-sized sand), yellowish white-colored ash (YA). The thickness is constant at 7–10 cm. YA was observed below OSC11 intercalated by a 2 cm thick peaty layer at Section B11. GA is a very well sorted (very fine sand to fine sand), greenish gray-colored ash layer of 3–6 cm in thickness. GA was recognized 50 cm below YA. The types of volcanic glass and mineral assemblages of YA and GA were determined based on microscopic identification. Glass shards of YA consist of 90% of bubble wall type and 10% of pumice type. The mineral assemblage of YA is plagioclase, pyroxenes, magnetite and hornblende. Although the type of glass shards of GA is primarily the same as that of YA, some of the bubble wall type exhibits a brownish color. The mineral assemblage of GA is plagioclase, pyroxenes and magnetite. Between the two ash layers,

Table 1
Characteristics of the major deposits in this study.

Unit	Facies	¹⁴ C age (BP)	Inferred age (ka BP)	Juvenile	Phenocryst							Thickness (cm)	Maximum grain size (mm)	Locality	Volume (km ³)	
					Type	Pl	Ol	Cpx	Opx	Hb	Bt					Qz
HPM1	pfa		0.7	WP ≫ BP	WP	++	-	+	-	++	+	-	16	40	A32	2 × 10 ⁻²
OSC1	sfa		>1.6	SC	SC	++	+	+	tr	-	-	tr	3	10	C04	3 × 10 ⁻²
OSC2	sfa			SC									1	2	C04	1 × 10 ⁻²
OSC3	sfa			SC									6	20	C04	6 × 10 ⁻²
OSC4	sfa			SC									5	6	C04	5 × 10 ⁻²
OSC5	sfa		3.2	SC									2	8	C04	2 × 10 ⁻²
HPM2	pfa	3320 ± 40		WP ≫ GP	WP	++	-	+	tr	++	-	-	22	60	B14	1 × 10 ⁻²
OSC6	sfa			SC	SC	+	+	+	-	-	-	-	4	4	A08	2 × 10 ⁻¹
OSC7	sfa		3.7	SC	SC	++	+	++	+	-	-	-	4	10	A08	3 × 10 ⁻²
HPM3	pfa		3.8	WP ≫ GP	WP	++	-	+	-	++	-	-	2	20	B14	2 × 10 ⁻⁴
OSC8	sfa		3.9	SC	SC	+	+	tr	-	-	-	-	7	2	A08	1 × 10 ⁻¹
OSC9	sfa		4	SC	SC	+	+	+	-	-	-	-	7	2	A08	7 × 10 ⁻²
OSC10	sfa		4	SC	SC								5	2	A08	1 × 10 ⁻¹
HPM4	pfa(?)		5.1	WP	WP	++	-	+	-	++	tr	-	22	120	B14	1 × 10 ⁻²
HPM5	pfa		5.8	WP ≫ GP	WP								17	25	B14	3 × 10 ⁻³
HPM6	pfa	6350 ± 30		WP ≫ BP,GP	WP	++	tr	+	-	++	-	-	45	40	B14	2 × 10 ⁻²
HPM7	pfa		6.8	WP ≫ GP	WP								2	7	B14	3 × 10 ⁻⁴
HPM8	pfa		7.2	WP	WP	++	-	-	-	++	-	-	8	15	B14	1 × 10 ⁻³
OSC11	sfa	7430 ± 40		SC	SC	+	+	+	-	-	-	-	10	10	A08	2 × 10 ⁻¹
YA	afa		7.6 ^a		ash	++	-	+	+	+	-	-	10	-	B06	
GA	afa	8540 ± 40			ash	++	-	+	+	-	-	-	6	-	B06	
Lomonosov	lava		8.5–9.5	Lava	LV	++	+	++	++	-	-	tr	>30 m		A01	2 × 10 ⁻¹
PPM1	pfl		9.5	WP ≫ Gp	WP	++	-	+	+	-	-	-	>60	3	C01	4 × 10 ⁻³
PPM2	pfa	9900 ± 50		WP	WP	++	tr	+	+	-	-	-	8	2	C01	4 × 10 ⁻³
PPM3	pfa		10.5	WP	WP	++	-	+	+	-	-	-	8	2.5	C01	4 × 10 ⁻³
Tatarinov proximal	pfa			WP>BP>SC	WP	++	-	++	++	-	-	-	>3 m	300	A14	
					WP	+	+	+	-	-	-	-				
					SC	++	tr	++	+	-	-	-				

Facies: afa, ash fall deposit; pfa, pumice fall deposit; pfl, pyroclastic flow deposit; sfa, scoria fall deposit. Type: WP, white pumice; BP, banded pumice; GP, gray pumice; SC, scoria and LV-lava. Phenocryst relative volumes: ++ > + > - > tr, trace.

^a Data from Ponomareva et al., (2004).

locally deposited ashes and several laminated reworked layers were interbedded. YA and GA ash layers are useful key beds because of their colors and uniform grain sizes and thicknesses in this area.

4.1.2. Lava flows and proximal deposits

4.1.2.1. Lava flows. The Lomonosov lava (Fig. 3) is covered by YA tephra intercalated by thick reworked deposits at Section B05 and overlies the PPM deposits at Section C01 (Fig. 5). In Section C01, more than 10 m of structureless lava flow with a clinker at the bottom (3 m thick) was recognized (Fig. 7). At the proximal area of Lomonosov, more than 3 m thick agglutinates were observed (Section C03), whose lithologies are the same as that of the Lomonosov lava. The majority of Lomonosov lava showed gray, pyroxene andesitic facies, occasionally including mafic enclaves about 2–5 cm in diameter. The phenocryst content is over 30 vol. % crystals, consisting of clinopyroxene, orthopyroxene and a very small amount of quartz and olivine.

On the slope of Fuss, three lava flows occurring at B12 and B13 are porphyritic and contain phenocrysts of plagioclase, hornblende, clinopyroxene, olivine and magnetite, with or without orthopyroxene. Stratigraphic relationships between these lavas and tephra layers were not observed.

4.1.2.2. Proximal deposits of the Tatarinov volcano. The moderately sorted pumice fall deposits, with thickness greater than 3 m, were preserved at the top of the Tatarinov summit crater wall, located about 3 km SSW of the Chikurachki summit (A14: Fig. 3). It consists of white pumice, banded pumice and small amount of scoria, up to 30 cm in diameter. White pumice and the white part of the banded pumice include pyroxene phenocrysts and plagioclase megacrysts (as large as 1 cm) with inclusions of olivine. Scoria and the darker

part of the banded pumice include olivine and clinopyroxene phenocrysts without orthopyroxene.

4.2. Correlation of tephra layers

Correlations of tephra layers were performed on the basis of combinations of geological and petrological data. HPM6, YA and GA can be considered as useful key beds for stratigraphic correlations in fieldwork. In addition, all tephra layers and selected organics-bearing layers were sampled at six type localities (A08, B14, B10, B15, C01 and C04) to determine their chemical signatures and radiocarbon dates, respectively. The petrological characteristics of each tephra are different, especially concerning glass chemistry (Tables 2 and 3). For example, the glass compositions of each tephra unit among the HPM series are clearly distinct in a K₂O–SiO₂ diagram (Fig. 12: see later discussion). These petrological features and additional radiocarbon dates allowed identification of each tephra layer at each site and determination of their correlations among different sites. Study confirmed the good continuity of many layers, including HPM1, 2 and 5 and OSC1–5 and 11 (Fig. 5).

5. Tephrochronology

AMS radiocarbon age determinations for peaty materials from seven stratigraphic levels at type localities were performed. Eruption ages of the HPM2, HPM6, OSC11 and PPM2 were directly obtained as 3320 ± 40, 6350 ± 30, 7430 ± 40, and 9900 ± 50 BP, respectively, using the peat and soil sampled directly beneath them (Table 4, Fig. 8). Although peat material was collected below the HPM1, originating from the youngest major eruption in this area, age data could not be obtained due to the presence of modern carbon. Beneath the HPM1, a locally recognized thin ash layer (Local

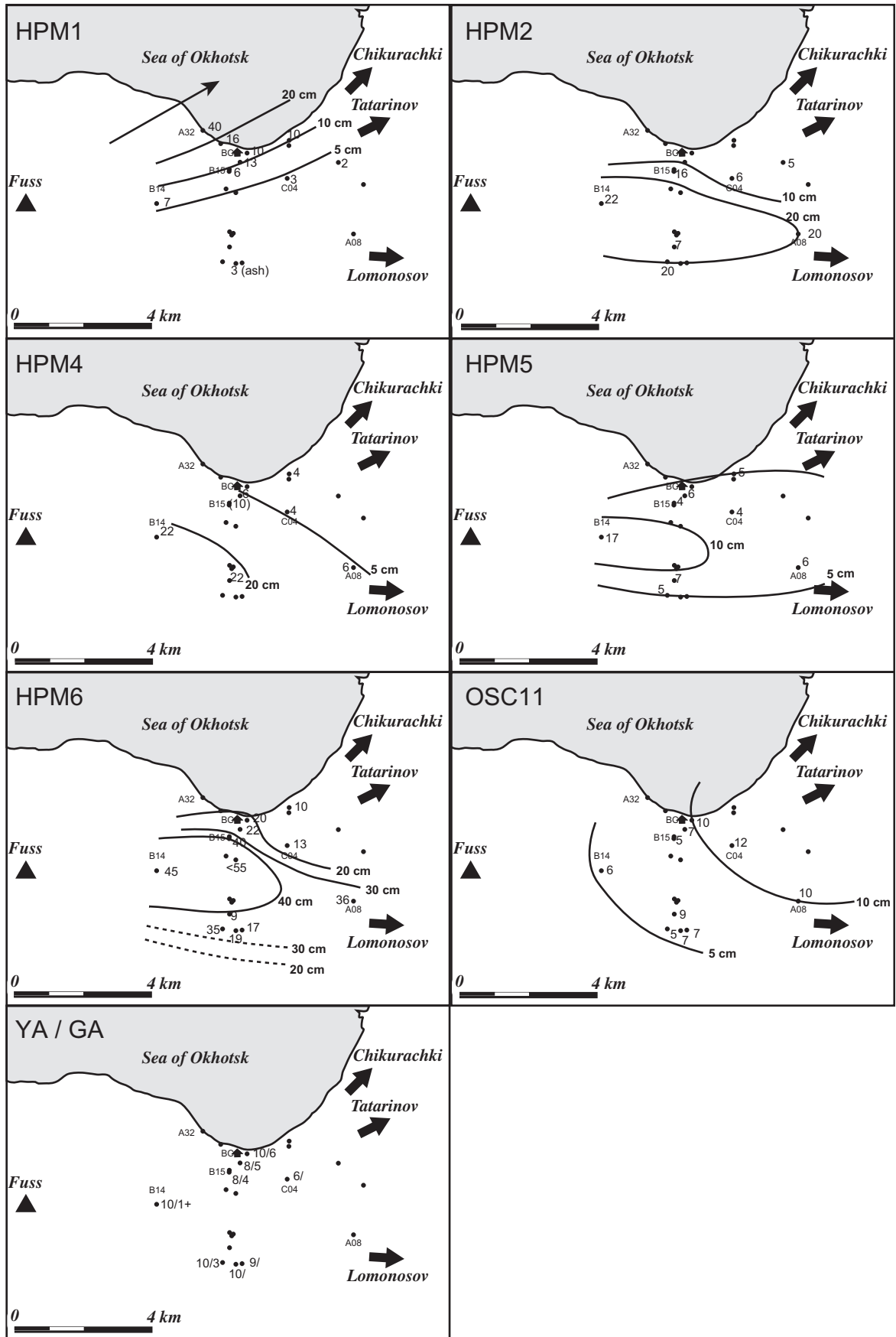


Fig. 6. Isopach maps of major eruptive units (HPM1, 2, 4, 5, 6, OSC11, and YA/GA). Directions of the summit of Chikurachki, Tatarinov and Lomonosov peaks are indicated by solid arrows.

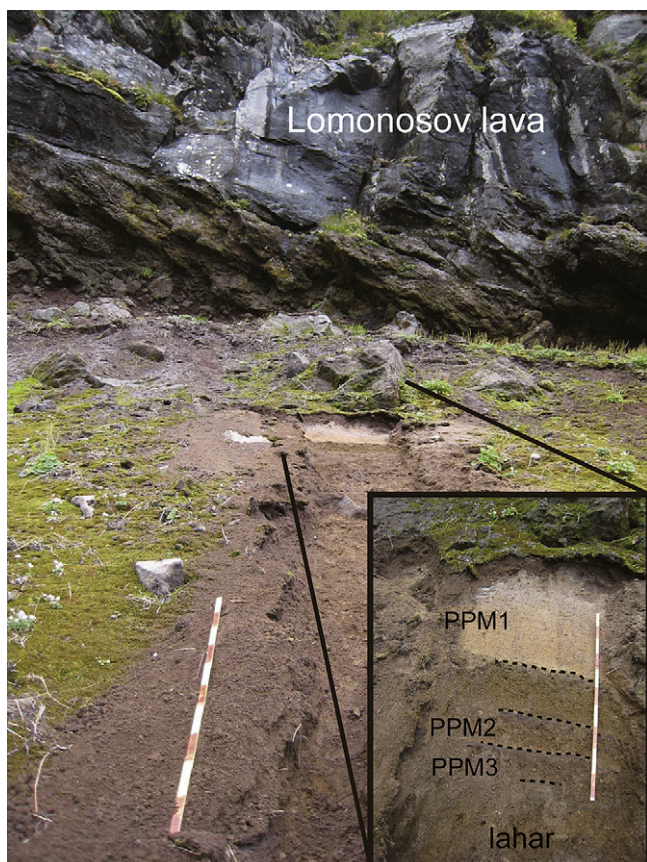


Fig. 7. Field occurrence of Lomonosov lava and underlying PPM series at C01. The scales of both photos are 1 m long.

ash-1) was recognized at B15. Dating of peat material below the Local ash-1 yielded 1650 ± 30 BP, indicating that the HPM1 is younger than 1650 BP. Based on the ages of the Local ash-1 and HPM2, the deposition age of OSC1–5 is estimated to be between 1650 ± 30 and 3320 ± 40 BP. The age of OSC6–10 ranges from 3320 ± 40 and 4700 ± 30 BP, using the soil layer above the HPM4 as dating material. Using the ages of HPM6 (6350 ± 30) and OSC11 (7430 ± 40), the ages of HPM4–5 and 7–8 can be estimated to range from 4700 ± 30 to 6350 ± 30 BP and from 6350 ± 30 to 7430 ± 40 BP (OSC11), respectively. The deposition age of the fine ash layer, GA, was newly dated at 8540 ± 40 BP from peat material directly below the layer. The Lomonosov lava, described as Holocene effusive deposits by Gorshkov (1970), might have been effused between 9900 ± 50 and 8540 ± 40 BP (Fig. 8).

6. Petrography and major elements chemistry

The Holocene eruptive deposits from this volcanic area can be petrographically divided into two main groups, the Hornblende-bearing Group (HPM series and Fuss lava) and the Hornblende-free Group (other tephra series and lavas of the CTL volcanic chain) (Table 5). The two groups also show different chemical variations. The whole-rock chemistry of Hornblende-free Group, including Pleistocene lavas sampled from the western foot of the volcanic chain, was classified as medium-K andesite according to Gill (1981) (Fig. 9). On the other hand, the Hornblende-bearing Group plotted near the field of high-K andesite in the SiO_2 – K_2O diagram. General petrological features of the two groups and two distal ash layers (YA and GA) are described here.

6.1. Hornblende-free group

The phenocryst content of juvenile materials of this group ranges from 19.6 to 36.1 vol.% (Table 5). Common phenocrysts of the group include plagioclase, clinopyroxene, orthopyroxene and opaque minerals. In addition, quartz phenocrysts showing resorption textures were recognized in Lomonosov lava and in scoria of the OSC series as a minor component. Olivine phenocrysts are common in the OSC scoria.

The whole-rock compositions of PPM and Tatarinov proximal ejecta range from 53 to 63 wt.% SiO_2 , and that of Lomonosov lava is 60–63 wt.% SiO_2 (mafic inclusions in the lava are about 54 wt.% SiO_2). In contrast, the scoria of OSC1–11 show more mafic composition of basaltic to basaltic andesite (49–55 wt.% SiO_2). Although these samples show a single linear trend in SiO_2 – K_2O , SiO_2 – CaO , SiO_2 – Rb and SiO_2 – Zr diagrams when graphed, they indicate clearly different trends on SiO_2 – MgO and Sr – Ba/Rb diagrams (Figs. 9 and 10). In the SiO_2 – MgO diagram, the rocks of each series (OSC, PPM and Lomonosov lava) form three distinct trends. The rocks of OSC show the lowest MgO values in the diagram at a similar SiO_2 content. In addition, OSC was classified as a tholeiitic series by Miyashiro (1974), whereas those of the Lomonosov lava were classified as a calc-alkaline series. The PPM and Tatarinov proximal ejecta were plotted along the boundary between two rock series (Fig. 9).

The glass compositions of scoria of the OSC series are andesitic, ranging from 55 to 62 wt.% SiO_2 . On the other hand, PPM and Tatarinov proximal ejecta show a wide range from 58 wt.% to 80 wt.% SiO_2 . Their compositions form a single linear trend in the SiO_2 – K_2O diagram, but they display different trends in the FeO – Al_2O_3 diagram (Fig. 11).

6.2. Hornblende-bearing group

The phenocryst contents of the rocks of this group are 13–19 vol.% in pumice and up to 34 vol.% in lava (Table 5). The common phenocryst assemblage of these rocks is plagioclase, hornblende, clinopyroxene and opaque minerals. Orthopyroxene phenocrysts are rarely contained in some of the pumice, and biotite phenocrysts are characteristically recognized in HPM1 and HPM4 pumice (Tables 1 and 5). Among the group, lava samples show various SiO_2 contents (52–61 wt.%), whereas white pumices are clustered more on the felsic side ($\text{SiO}_2 > 58$ wt.%) (Fig. 9).

The rocks of the group were classified into the calc-alkaline andesite series on the SiO_2 – FeO/MgO diagram (Miyashiro, 1974). Compared with the rocks of the Hornblende-free group, these rocks are also richer in incompatible trace elements (when at similar SiO_2 content), such as Zr, Rb and Ba (Fig. 10). In addition, the glass composition of the HPM series is characterized by higher K_2O and lower FeO^* contents (Fig. 11). Gray pumices contained in the HPM series show lower silica contents (<70 wt.% SiO_2 in glass composition) than white pumice of the same layer. Compositional fields of glass chemistries for white pumices of each HPM were distinguished on the K_2O – SiO_2 diagram (Fig. 12). Pumice samples in HPM3 show relatively low silica (69–71 wt.%) and high- K_2O contents (5.1–5.6 wt.%) at a given SiO_2 among the HPM series. K_2O contents of HPM1 and HPM4, which are characterized by containing biotite phenocrysts, are also higher (HPM1: 4.8–5.5 wt.%; HPM4: 5.7–6.3 wt.%), and HPM4 is particularly the most felsic ($\text{SiO}_2 = 74$ –77 wt.%). On the other hand, the K_2O value of HPM2 is the lowest ($\text{SiO}_2 = 72$ –74 wt.%, $\text{K}_2\text{O} = 3.7$ –4.2 wt.%). Although compositions of older sequential units of HPM6–8 overlap, this cluster shows individual field. HPM5 is also identifiable because of the unique compositional field ($\text{SiO}_2 = 74$ –76 wt.%; $\text{K}_2\text{O} = 4.3$ –4.7 wt.%) near the fields of HPM2 and HPM6–8.

Table 2
Major element compositions of volcanic glass for selected samples.

Sample no.	A08-01-01	B14-06a	A08-11	B14-01A	B14-04	B15-20	B14-10B	A08-16	B14-13	B14-14	B14-15	A14-01	A14-04 ^a	A14-05	C01-01B	C01-04	C01-05	B15-52	B15-61
Unit	OSC1–5	OSC6	OSC9	HPM1	HPM2	HPM3	HPM4	HPM5	HPM6	HPM7	HPM8	Ta. Tephra	Ta. Tephra	Ta. Tephra	PPM1	PPM2	PPM3	YA	GA
Type	SC	SC	SC	WP	WP	WP	WP	WP	WP	WP	WP	WP	SC	GP	WP	WP	WP	ash	ash
Locality	A08	B14	A08	B14	B14	B15	B15	A08	B14	B14	B14	A14	A14	A14	C01	C01	C01	B15	B15
Source	Ck	Ck	Ck	Fu	Fu	Fu	Fu	Fu	Fu	Fu	Fu	Ta	Ta	Ta	Ta or Lo	Ta or Lo	Ta or Lo	KO	??
Average wt.%																			
SiO ₂	60.31	58.90	59.98	72.99	72.73	70.04	75.24	74.36	73.49	73.24	73.31	76.10	59.84	68.30	78.48	62.52	69.75	77.26	74.14
TiO ₂	1.20	1.36	1.53	0.27	0.27	0.46	0.34	0.26	0.27	0.26	0.14	0.42	0.89	0.79	0.48	0.93	0.72	0.24	0.43
Al ₂ O ₃	16.19	15.69	14.24	14.49	14.78	15.47	12.96	13.97	14.56	14.64	14.87	12.64	17.43	14.82	11.03	16.50	13.85	13.07	13.41
Fe ₂ O ₃	8.66	9.75	9.77	1.57	1.85	2.29	1.24	1.44	1.35	1.44	1.22	1.99	6.68	4.93	1.67	6.49	4.41	1.46	3.81
MnO	0.19	0.16	0.18	0.12	0.12	0.12	0.11	0.12	0.09	0.14	0.06	0.07	0.24	0.12	0.02	0.14	0.11	0.07	0.13
MgO	2.20	3.00	2.02	0.40	0.51	0.64	0.35	0.34	0.28	0.29	0.18	0.40	2.87	1.36	0.21	2.22	1.07	0.31	0.65
CaO	6.16	6.81	5.63	1.51	1.90	1.74	0.83	1.38	1.61	1.65	1.72	1.47	5.50	3.52	0.75	5.49	3.45	1.42	2.64
Na ₂ O	3.46	3.02	5.02	3.43	3.87	3.83	3.00	3.70	3.77	3.77	3.92	3.57	4.21	3.60	3.09	3.74	3.72	4.07	3.86
K ₂ O	1.64	1.32	1.64	5.21	3.96	5.41	5.94	4.44	4.60	4.58	4.58	3.34	2.34	2.57	4.28	1.97	2.92	2.09	0.93
n	16	20	13	20	15	10	14	8	10	10	10	10	10	9	10	10	10	10	10
St. dev.																			
SiO ₂	0.91	1.21	0.73	0.96	0.36	0.19	0.49	0.65	0.16	0.72	0.54	0.30	0.55	0.42	0.63	1.73	0.25	0.31	0.46
TiO ₂	0.19	0.28	0.14	0.08	0.07	0.06	0.05	0.07	0.07	0.10	0.11	0.06	0.09	0.10	0.08	0.18	0.10	0.05	0.09
Al ₂ O ₃	1.69	2.06	1.24	0.36	0.27	0.08	0.36	0.27	0.08	0.52	0.54	0.11	0.47	0.23	0.48	2.31	0.32	0.13	0.12
Fe ₂ O ₃	1.34	1.33	1.03	0.25	0.11	0.16	0.20	0.15	0.15	0.14	0.13	0.16	0.60	0.22	0.12	1.10	0.29	0.21	0.14
MnO	0.15	0.11	0.11	0.08	0.09	0.10	0.11	0.12	0.07	0.06	0.07	0.11	0.14	0.09	0.10	0.10	0.14	0.07	0.09
MgO	0.68	0.55	0.21	0.12	0.07	0.06	0.14	0.06	0.05	0.06	0.06	0.04	0.42	0.10	0.07	0.76	0.09	0.03	0.04
CaO	0.82	0.74	0.52	0.21	0.09	0.09	0.16	0.17	0.06	0.21	0.17	0.09	0.25	0.14	0.28	0.96	0.18	0.07	0.09
Na ₂ O	0.22	0.40	0.36	0.17	0.15	0.09	0.12	0.06	0.06	0.18	0.20	0.09	0.11	0.12	0.09	0.28	0.11	0.08	0.23
K ₂ O	0.23	0.27	0.15	0.18	0.11	0.09	0.16	0.10	0.10	0.19	0.19	0.04	0.12	0.13	0.25	0.37	0.07	0.14	0.06

Ck, Chikurachki; Fu, Fuss; Lo, Lomonosov; Ta, Tatarinov; and KO, Kurile Lake caldera; n, number of analysis; st. dev., standard deviation. See the caption of Table 1 for the other abbreviations.

^a Broad beam analysis (probe dimensions = 10–50 μm).

Table 3
Whole-rock compositions of major and trace elements.

Sample no.	A08-01A ^a	A08-08A ^a	B15-03C	B15-15B ^a	B15-20B ^a	B15-35 ^a	B15-43B ^a	B12	B13-01	A30-01	A01	C03	C02-01	A14-01	A14-04	A14-05	A15	A05	A11	A17	A22-03
Unit	OSC1–5	OSC7	HPM1	HPM2	HPM3	HPM4	HPM6	Fu. L1	Fu. L2	Fu. BA	Lo. L1	Lo. Ag.	Lo. Dome	Ta. Tephra	Ta. Tephra	Ta. Tephra	Ta. Tephra	A05 L	A11 L	A17 L	A22 L3
Occurrence	Scoria	Scoria	WP	WP	WP	WP	WP	Lava	Lava	Lava block	Lava	Ag	Lava block	WP	Scoria	GP	Lava block	Lava	Lava	Lava	Lava
Locality	A08	A08	B15	B15	B15	B15	B15	B12	B13	A30	A01	C03	C02	A14	A14	A14	A15	A05	A11	A17	A22
Source	Ck	Ck	Fu	Fu	Fu	Fu	Fu	Fu	Fu	Fu	Lo	Lo	Lo	Ta	Ta	Ta	Ta	Oc	Oc	Oc	Oc
wt.%																					
SiO ₂	52.02	51.27	59.90	58.17	57.25	60.76	60.18	55.15	56.02	60.29	60.19	62.09	60.56	62.30	55.26	57.15	54.50	57.41	62.72	53.21	53.84
TiO ₂	0.81	0.92	0.55	0.55	0.65	0.52	0.53	0.70	0.67	0.50	0.61	0.60	0.63	0.63	0.87	0.76	0.74	0.72	0.75	0.76	0.79
Al ₂ O ₃	20.94	20.11	17.61	18.08	17.47	17.72	17.98	17.62	17.60	17.49	16.21	16.60	16.37	16.86	17.93	17.78	18.42	17.64	17.47	21.54	19.17
Fe ₂ O ₃	9.70	11.01	6.65	7.09	7.32	5.21	6.32	8.08	7.85	6.04	7.28	6.61	6.91	6.36	9.48	8.89	9.14	8.57	6.39	8.31	9.48
MnO	0.17	0.21	0.17	0.20	0.18	0.17	0.20	0.17	0.17	0.17	0.17	0.15	0.16	0.17	0.20	0.18	0.18	0.19	0.19	0.17	0.19
MgO	4.17	4.62	2.77	2.90	3.01	2.41	2.43	4.60	4.47	2.31	4.01	2.82	2.82	2.33	4.14	3.81	4.71	3.63	1.99	3.15	4.21
CaO	9.72	10.13	6.94	7.26	7.00	6.91	6.58	9.33	8.69	6.72	7.40	6.59	6.83	6.17	8.79	8.15	8.98	7.87	5.55	10.23	9.16
Na ₂ O	2.60	2.70	3.43	3.48	3.38	3.47	3.64	2.98	3.02	3.52	3.08	3.32	3.30	3.68	3.20	3.14	2.92	3.19	4.47	3.05	2.85
K ₂ O	0.74	0.47	2.72	1.99	2.71	2.82	2.39	2.05	2.17	2.80	1.66	1.79	1.81	1.72	1.13	1.19	0.97	1.29	1.41	0.77	0.62
P ₂ O ₅	0.18	0.17	0.24	0.30	0.18	0.29	0.30	0.25	0.27	0.28	0.14	0.16	0.16	0.19	0.19	0.17	0.16	0.18	0.34	0.20	0.18
Total	101.03	101.61	100.97	100.03	99.13	100.27	100.55	100.92	100.92	100.13	100.75	100.73	99.54	100.41	101.19	101.23	100.71	100.69	101.27	101.37	100.47
ppm																					
Sc	26	35	16	17	19	12	14	30	24	12	25	20	21	21	33	31	26	23	18	25	22
V	274	336	181	166	207	152	166	299	252	149	209	181	191	162	354	285	283	221	103	245	252
Cr	9	8	9	8	5	6	4	51	43	3	56	17	11	5	9	7	17	10	2	7	6
Co	28	32	20	20	22	15	18	25	25	18	23	20	20	19	30	28	30	26	17	26	27
Ni	9	8	7	6	5	4	4	20	22	4	30	11	7	3	6	6	20	8	3	6	5
Cu	92	113	49	27	43	30	18	67	64	41	55	56	50	46	107	110	84	72	31	108	52
Rb	15	10	75	51	71	78	62	49	52	76	34	37	36	36	24	26	18	27	26	16	10
Zn	63	78	79	87	78	71	84	71	69	74	64	61	63	65	85	73	69	68	68	71	52
Sr	499	494	552	661	542	582	648	526	536	586	406	405	403	423	469	437	451	478	501	527	566
Y	22	21	20	23	20	24	22	19	20	22	25	26	27	30	26	24	21	26	38	22	21
Zr	61	47	118	100	124	125	112	87	92	122	100	112	107	109	72	81	65	78	97	57	43
Nb	2	2	2	2	2	3	2	2	2	2	3	3	2	3	2	2	2	2	3	2	1
Ba	199	145	553	556	572	578	684	435	454	602	373	413	437	426	278	305	229	317	403	240	233
Pb	5	4	8	8	7	7	6	5	7	7	6	7	9	9	5	7	7	4	7	4	5
Th	3	3	9	9	7	8	8	9	11	8	6	2	2	3	1	2	1	2	2	2	1
Ga	17	18	19	19	17	16	20	14	18	19	16	14	15	16	20	19	13	17	15	18	14
La	5	3	15	14	11	20	15	10	9	18	10	10	7	11	3	6	4	9	14	8	8
Ce	15	14	39	38	35	46	42	29	29	40	28	33	30	32	24	24	18	22	33	15	10

Oc, old lava from the Chikurachki group; Ag, agglutinate; BA, block and ash flow deposit. See the caption of Tables 1 and 2 for the other abbreviations.

^a Multi-grain analysis.

Table 4
Sample information and analytical results of radiocarbon dating.

Sample	Stratigraphic position	Loc.	Lab. Code	Method	Material	¹⁴ C age (BP)	δ ¹³ C (permil)	Calender age 1 sigma range
B11-02	Just below HPM1	B11	IAAA-72596	AMS	Peat	Modern	-29.0	
B15-09	10 cm above OSC 1	B15	IAAA-72947	AMS	Peat	1650 ± 30	-21.74	345–370 AD (13.1%) 375–430 AD (55.1%)
B10-05	Just below HPM 2	B10	IAAA-72594	AMS	Peat	3320 ± 40	-26.6	1660–1650 BC (1.0%) 1640–1520 BC (67.2%)
B15-32	5 cm above HPM 4	B15	IAAA-72948	AMS	Peat	4700 ± 30	-21.82	3530–3490 BC (16.1%) 3450–3370 BC (44.6%)
B15-44	Just below HPM 6	B15	IAAA-72597	AMS	Peat	6350 ± 30	-23.5	5365–5305 BC (68.2%)
B10-22	Just below OSC11	B10	IAAA-72595	AMS	Peat	7430 ± 40	-25.4	6370–6240 BC (68.2%)
B15-62	Just below GA	B15	IAAA-72598	AMS	Peat	8540 ± 40	-25.1	7595–7550 BC (68.2%)
C01-06	Just below PPM 2	C01	IAAA-72599	AMS	Soil	9900 ± 50	-27.5	9440–9430 BC (2.0%) 9400–9280 BC (66.2%)

Error ranges of ¹⁴C age are 2 sigma.

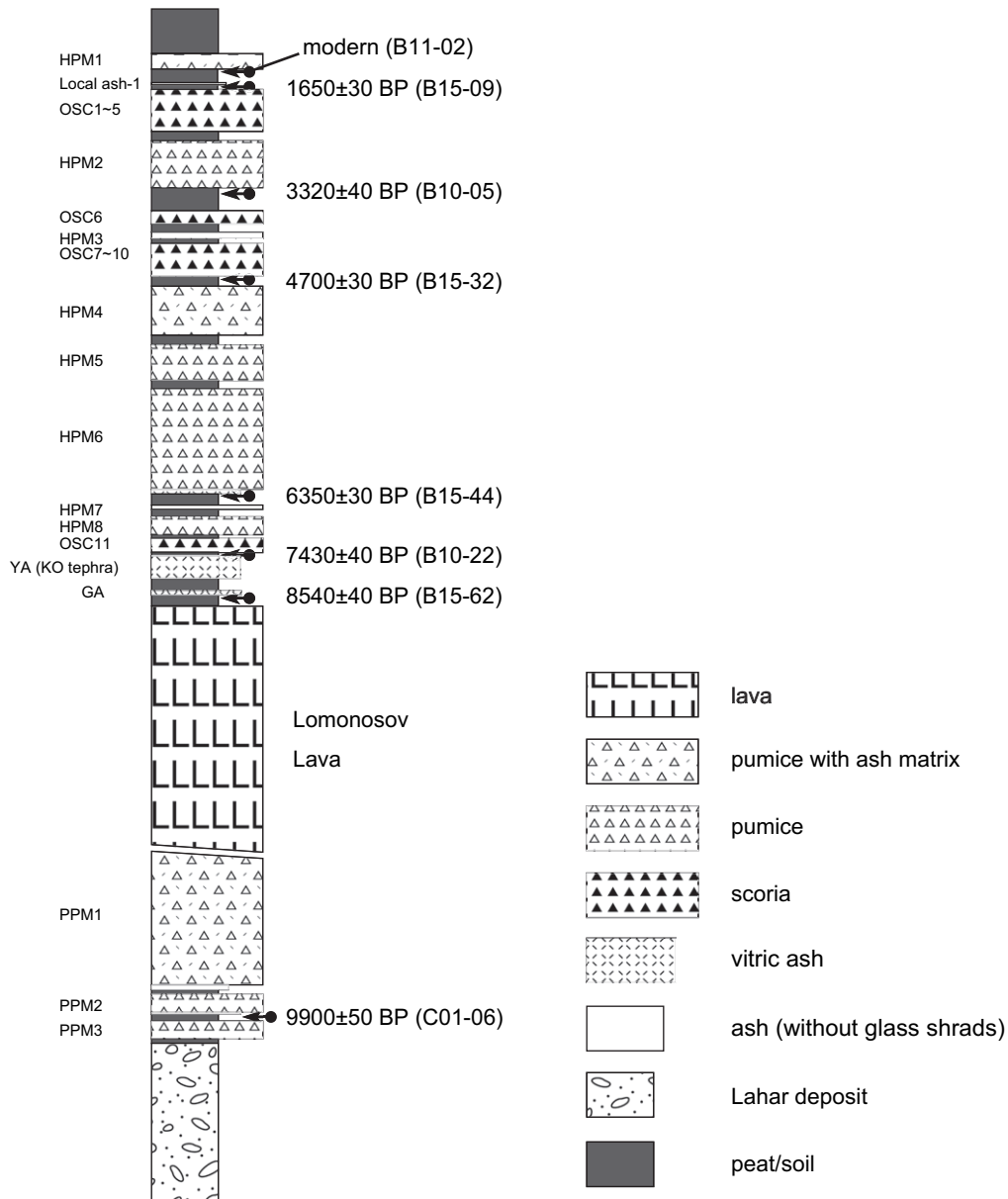


Fig. 8. Summary section of major tephra layers in the studied area.

Table 5
Modal compositions of volcanic rocks from each eruption unit.

Sample no.	Unit	Type	Locality	Crystal content	Gm	Pl	Ol	Cpx	Opx	Hb	Bt	Qz	Opq
B14-01B	HPM1	White pumice	B14	13.9	86.1	9.1	–	0.6	–	3.4	0.3	–	0.4
B14-04	HPM2	White pumice	B14	18.6	81.4	10.5	–	1.0	Trace	5.8	–	–	1.3
B14-13	HPM6	White pumice	B14	17.8	82.2	12.0	Trace	0.2	–	4.9	–	–	0.7
B13-01	Fuss	Lava	B13	34.0	66.0	25.5	0.1	4.9	1.2	0.5	–	–	1.7
B15-10B	OSC1–5	Scoria	B15	27.7	72.3	26.5	0.7	0.1	Trace	–	–	Trace	0.2
A08-08	OSC7	Scoria	A08	19.6	80.4	13.3	1.0	4.1	0.2	–	–	–	0.9
A14-03	Tatarinov	Scoria (proximal)	A14	25.6	74.4	21.6	Trace	2.5	0.8	–	–	–	0.6
A14-08	Tatarinov	Pumice (proximal)	A14	21.0	79.0	14.7	–	1.8	3.6	–	–	–	0.9
A01	Lomonosov	Lava	A01	36.1	63.9	24.1	0.2	7.9	2.8	–	–	Trace	1.0
A03	Lomonosov	Lava	A03	33.3	66.7	26.9	–	3.5	1.3	–	–	Trace	1.5

6.3. Distal ash layers

Although the mineral assemblage of the two fine ash layers (YA and GA) is the same as that of the Hornblende-bearing Group, the glass chemistry of YA and GA is clearly distinct from that of the Hornblende-bearing and Hornblende-free Groups. At a similar SiO₂ content, the K₂O contents of YA and GA were lower than those of the other tephra layers (Fig. 11). GA displays the lowest K₂O content (0.8–1.1 wt.% K₂O and 73–75 wt.% SiO₂), whereas YA was plotted in the intermediate field (1.8–2.4 wt.% K₂O, and 76–78 wt.% SiO₂) between GA and Tatarinov ejecta in the SiO₂–K₂O diagram.

7. Discussion

7.1. Correlation between tephra units and source volcano

7.1.1. OSC, HPM and PPM layers

Four lithological tephra series were described in this area. The thicknesses of pumice fall deposits of the HPM series (HPM1, 2, 4, 5 and 6) increases remarkably towards the Fuss peak (Fig. 5). In particular, isopach maps of HPM2, 5 and 6 clearly indicate eastern dispersal axes extending from the Fuss peak (Fig. 6). Other pumice fall deposits of HPM series (HPM3, 7 and 8) were found only at the eastern periphery of Fuss. These geological data suggest that the HPM tephra were derived from Fuss and deposited on the eastern side by westerly winds. The previously reported petrography and whole-rock composition of pumiceous andesite bomb, sampled at Fuss peak (Gorshkov, 1970), are the same as those of the HPM tephra with respect to their hornblende-rich phenocryst assemblage and high-K₂O content within andesitic composition (K₂O = 1.5–3.2 wt.%, SiO₂ = 52–63 wt.%; Fig. 13). In addition, lava flows sampled at the edifice of Fuss in this study also show the same characteristics (hornblende-rich and high potassium composition) as those of HPM tephra. These petrological data also strongly indicate that HPM tephra were from Fuss rather than the CTL volcanic chain, which has issued hornblende-free, medium-K basaltic to andesitic magmas (e.g., Gorshkov, 1970, Bailey et al., 1989).

Although both of the OSC and PPM series were considered to be emitted from the CTL volcanic chain when based on the field evidence, the petrological difference between the two series could indicate their distinct source volcanoes in the volcanic chain. Maximum grain size, thickness and the number of layers of other OSC series increase towards the CTL volcanic chain (Fig. 5). The isopach map of OSC11 suggests that it might be from Chikurachki or Tatarinov (Fig. 6). The chemical trends of glass shards and whole-rock of the OSC series, showing relatively mafic compositions (SiO₂ = 55–62 wt.% and FeO* = 4–13 wt.% in glass chemistry; SiO₂ = 49–53 wt.% in whole-rock chemistry), are inconsistent with those of Tatarinov proximal ejecta and Lomonosov lava but were consistent with the historical and prehistorical (that is ancient)

scoria fall deposits from Chikurachki reported by Gurenko et al. (2005) and Belousov et al. (2003) (Figs. 11, 13, and 16). The reported petrography of Chikurachki scoria (Gorshkov, 1970; Gurenko et al., 2005) characterized by olivine phenocrysts (uncommon in Tatarinov and Lomonosov) is also consistent with the OSC mineral assemblages.

On the other hand, the glass chemistry of proximal ejecta of the Tatarinov summit crater rim (A14) overlap well with those of the PPM tephra series on the diagrams (Fig. 11). In addition, the chemical composition of whole-rock samples of the Tatarinov proximal ejecta and Lomonosov lava also overlap with those of the PPM series. The phenocryst assemblages comprising clinopyroxene ± olivine are similar among the Tatarinov proximal ejecta, Lomonosov lava and PPM tephra. These petrological correlations suggest that PPM tephra series are the products of Tatarinov or Lomonosov rather than of Fuss or Chikurachki.

7.1.2. Distal ash layers

Field occurrences of the two ash layers (YA and GA), including fine-grained facies and uniformity in their thickness, strongly indicate that YA and GA are widespread tephra from distal volcanoes. The chemical compositions of the glass shards of the two layers also differ from the eruptive products of volcanoes in this volcanic area, particularly in the SiO₂–K₂O diagram. This also suggests distal source volcanoes for YA and GA.

The glass composition and phenocryst assemblage of YA (plagioclase, clinopyroxene, orthopyroxene and hornblende) are the same as those of the “KO tephra”, which has unique petrological features in common with other Kamchatkan volcanoes (Braitseva et al., 1995; Ponomareva et al., 2004). The tephra erupted from the Kurile Lake caldera in southern Kamchatka (Zaretskaia et al., 2001; Ponomareva et al., 2004). The obtained ¹⁴C age for peat layers bracketing YA (Fig. 8) (7430 ± 40 BP, from below OSC11 at B10; 8540 ± 40 BP, from below GA at B15; Table 4) agree with the age of the KO tephra (7.6 ka BP; Zaretskaia et al., 2001; Ponomareva et al., 2004). Furthermore, the thickness of YA in this studied area, approximately 10 cm, is consistent with the reported isopach map of the KO tephra drawn by Ponomareva et al. (2004). This evidence suggests that YA can be correlated with the KO tephra from the Kurile Lake caldera. Although GA might be generated from the other caldera-forming eruption, it is difficult to determine the source volcano because of inadequacy of the tephra-stratigraphic and petrologic studies for the volcanoes in the Kurile Islands. However, the two layers including GA could be good time markers of the early Holocene in the Kurile Islands and Kamchatka.

7.2. Estimation of eruption age and volume

7.2.1. Eruption age

The eruption ages of the tephra layers also were determined by using the accumulation rate of the peat and/or soil layers bracketed

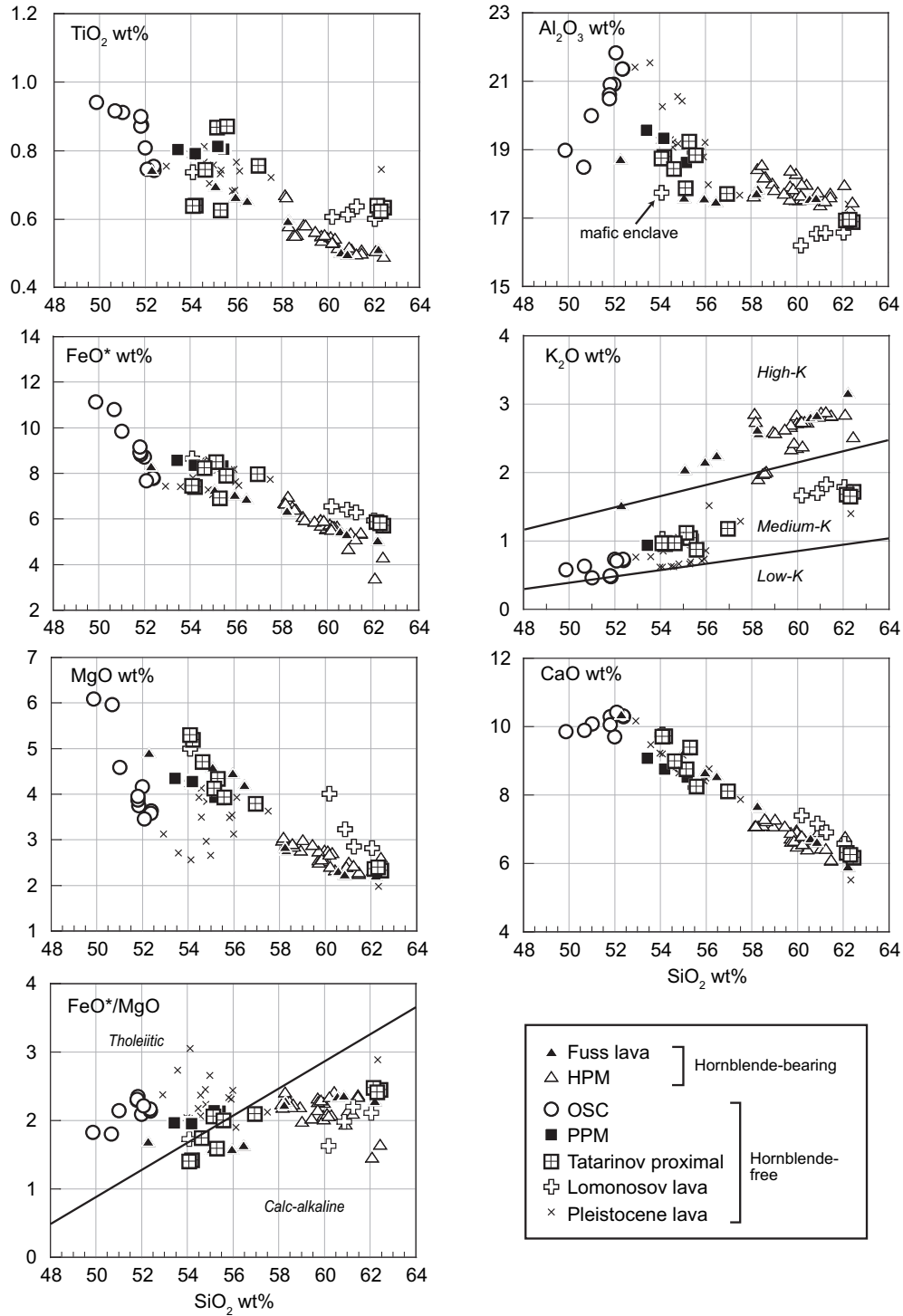


Fig. 9. Harker diagrams of whole-rock chemistry for major elements. Compositional boundaries on K₂O and FeO*/MgO Harker diagrams are drawn based on Gill (1981) and Miyashiro (1974), respectively.

by ¹⁴C dated horizons (e.g., Clark et al., 2006). The regression line between the dated age and cumulative thicknesses of soil/peat shows good linearity during 8–2 ka BP at Sites B10 and B15 (Fig. 14). This implies that the depositional rate of soil/peat was constant at the same location during 8–2 ka BP. The accumulation rates at B10 and B15 are about 35 cm/ky and 8 cm/ky, respectively. The high rate at B10 is possibly due to the marshy condition. These rates enable estimation of the eruption age for HPM5 (shown in

Fig. 14a) and HPM3, 4, 5 and 8 (shown in Fig. 14b). In this way, the ages of OSC1–10 described at B15 can also be estimated. The regression line between the stratigraphic levels of GA and the Local ash-1 could not be extrapolated towards the modern age (Fig. 14a). This reflects the change of depositional conditions and/or an inadequate compaction after 2 ka BP, and so the measurement for the peat below HPM1 does not indicate the age. According to the line between the Local ash-1 and the surface, the age of HPM1 is

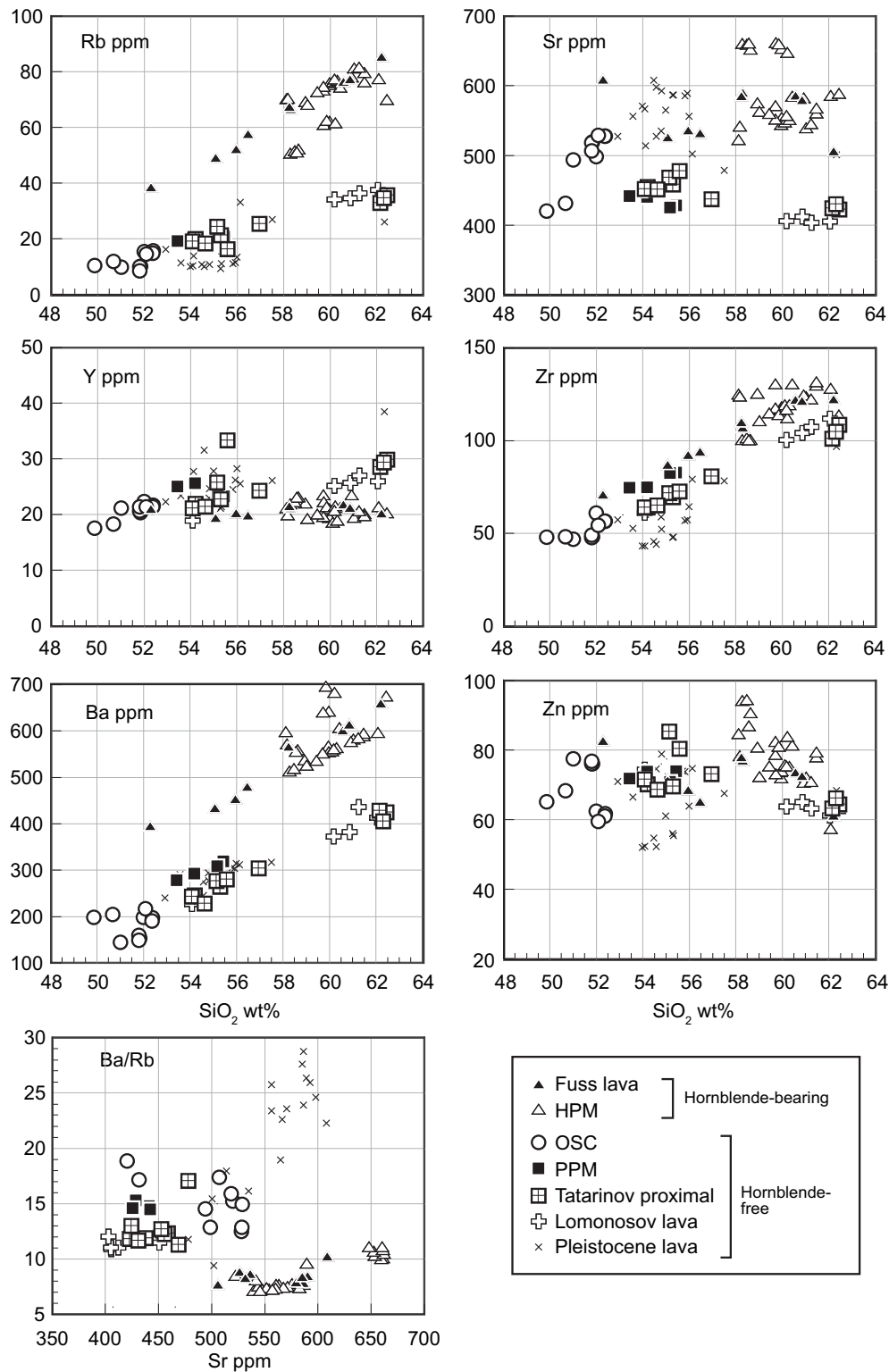


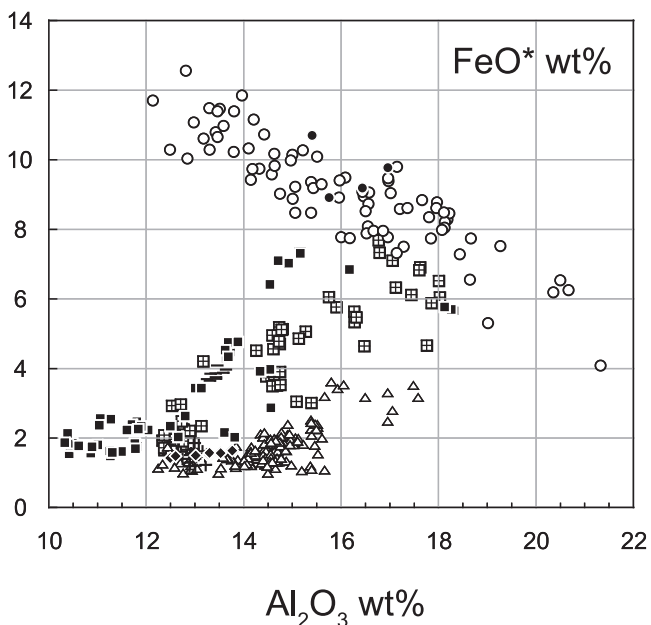
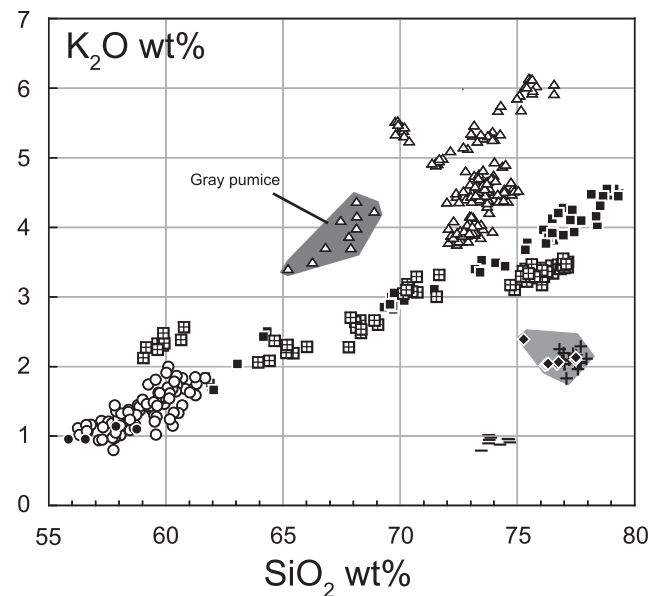
Fig. 10. Harker diagrams of whole-rock chemistry for trace elements.

roughly estimated to be 0.7 ka BP. As a consequence, the eruption ages of all of the tephra layers identified in the studied area could be determined.

7.2.2. Eruptive volume

The area of the tephra sections is located on the leeward side of Fuss or the windward side of the CTL volcanic chain. Thus, the

eruptive volume of each eruption from Fuss could be obtained by isopach maps of each tephra. In the case of HPM2, 5 and 6, these isopach maps (shown in Fig. 6) were extrapolated to calculate each eruptive minimum volume using the method of Legros (2000). Calculated volumes of HPM2, 5 and 6 are about 0.014, 0.0035 and 0.021 km³, respectively. Although isopach maps of other tephra layers from Fuss have not been obtained, the volume of each of



- Olivine-pyroxene scoria (OSC)
- △ Hornblende pumice (HPM)
- Pyroxene pumice (PPM)
- ▣ Tatarinov proximal ejecta
- + Yellow ash (YA)
- Green ash (GA)
- ◆ KO tephra (Ponomareva et al., 2004)
- Chikurachki scoria (Gurenko et al., 2005)

Fig. 11. Selected variation diagrams (K_2O-SiO_2 and $FeO^*-Al_2O_3$) for glass composition of juvenile materials and glass shards from tephra layers. Referenced data of the KO tephra (Ponomareva et al., 2004) and Chikurachki scoria (Gurenko et al., 2005) are shown for correlation.

these layers can be roughly estimated by using the thickness ratio to the volume determined layer (HPM2, 5 and 6) at the same locality as follows: $HPM1 = 0.02 \text{ km}^3$, $HPM3 = 0.0002 \text{ km}^3$, $HPM4 = 0.01 \text{ km}^3$, $HPM7 = 0.0003 \text{ km}^3$ and $HPM8 = 0.001 \text{ km}^3$. These estimations could indicate the VEI (Volcano Explosive Index by Newhall and Self, 1982) < 3 for each eruption.

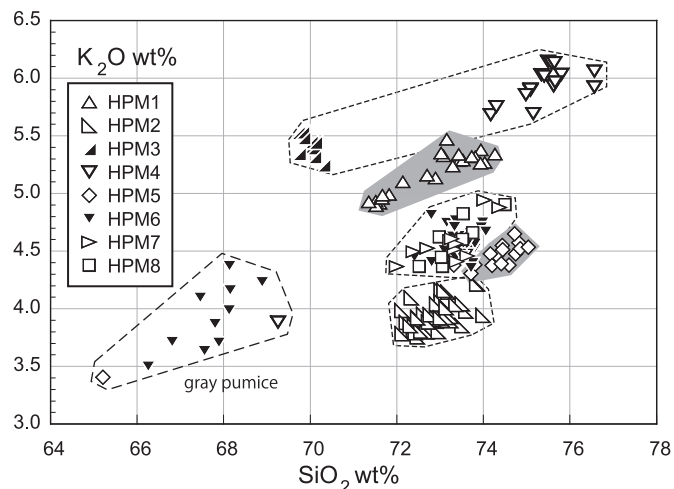


Fig. 12. K_2O-SiO_2 variations for glass chemistry of HPM1–8.

In contrast, tephra from the CTL volcanic chain would usually be distributed at the eastern flank of the chain. Thus, the studies at the western flank of the volcano would miss many of eruptive deposits of the volcano. For example, only five thin volcanic sand layers (OSC1–5) were identified in the southwestern flank of Chikurachki volcano during the latest 3320 years, and no recent eruptive deposits of the volcano were found, including the 1853 and 1986 eruptions noted by Belousov et al. (2003) (Fig. 15). Belousov et al. (2003) described the recent tephra sections at the eastern-southeastern flank of Chikurachki, in which more than 10 tephra layers occur, including those from the 1853 and 1986 eruptions and many thick and coarse scoria fall deposits (Fig. 15). The volumes of the 1853 and 1986 major historical eruptions were estimated to be 0.09 and 0.12 km^3 respectively (Belousov et al., 2003), using the method of Fierstein and Nathenson (1992). The reported volume of 1853 tephra (0.09 km^3) was recalculated at approximately 0.06 km^3 , using the Legros (2000) method from the Belousov et al. (2003) isopach without changing order. They did not, however, estimate the age of the lower layers recognized at each section. At Section 0 of Belousov et al. (2003), located 5.4 km NE from the Chikurachki summit (star in Fig. 3), they identified a soil layer (5 cm) between the 1853 layer and the underlying layers (Fig. 15). The underlying layer was considered slightly older than AD 1793. Assuming a major historic eruption (AD 1793) produced the underlying layer before AD 1853, the soil accumulation rate between the above two layers was calculated as less than 50 cm/ky . Considering the total thickness (more than 1 m in Fig. 15) and compaction of soil layers, the deposition age of the lowermost tephra (Tephra1 in Fig. 15) at Section 0, defined as the “ancient tephra” by Belousov et al. (2003), was estimated as older than 2 ka BP . The estimated soil accumulation rate must be overestimated, suggesting that the lowermost tephra is much older and is around $2-4 \text{ ka BP}$. This indicates that the recognized lowermost layer at the eastern flank of the volcano may be correlated with one of OSC1–5 at the western flank.

The MgO content of the Chikurachki scoria decreased temporally with slightly increasing SiO_2 content (Fig. 16). The Tephra1 scoria (Fig. 15) have similar SiO_2 and MgO contents as those of the OSC1–5 (Fig. 16) that were effused during $3.3-1.6 \text{ ka BP}$. By combining the age constraint and this temporal chemical change, the Tephra1 could be correlated to one of the layers of OSC1–5. Tephra1 was considered comparable to or larger in size than the 1853 tephra (0.09 km^3) because the thickness and grain size of Tephra1 is as large as those of the 1853 tephra at the eastern flank

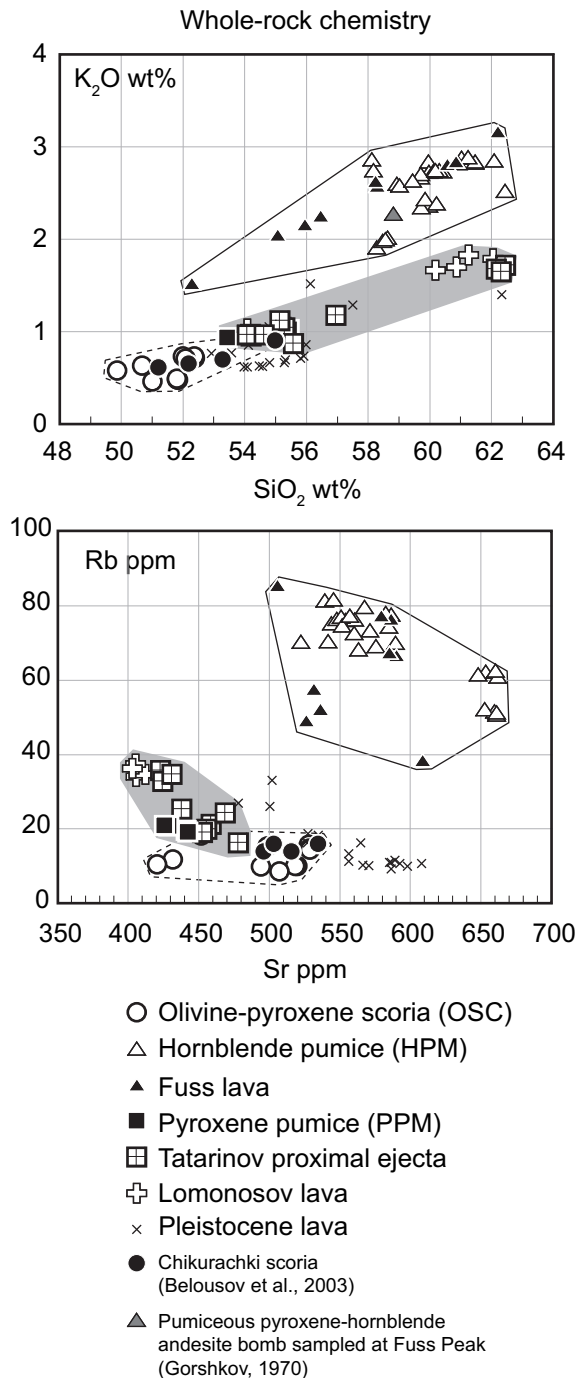


Fig. 13. Whole-rock compositions (K_2O – SiO_2 and Rb – Sr variations) of tephras and lavas. The reported analytical data of the Chikurachki scoria (Belousov et al., 2003) and the Fuss pumiceous bomb (Gorshkov, 1970) are also plotted for correlation.

(Fig. 15; Belousov et al., 2003). Considering the difference of volume estimation methods between Belousov et al. (2003) and this study, the volume of Tephra1 could be estimated to be about 0.06 km^3 . If Tephra1 could be correlated with OSC3, the thickest (0.06 m thick) among OSC1–5 (Table 1), the volume of each of the other OSC tephra layers would be roughly determined using thickness ratio to the OSC3 at the same locality (C04; Table 1; Fig. 5) as follows: OSC1 = 0.03 km^3 , OSC2 = 0.01 km^3 , OSC4 = 0.05 km^3 , OSC5 = 0.02 km^3 , OSC6 = 0.15 km^3 , OSC7 = 0.03 km^3 , OSC8 = 0.10 km^3 , OSC9 = 0.07 km^3 , OSC10 = 0.10 km^3 and OSC11 = 0.18 km^3 . Although

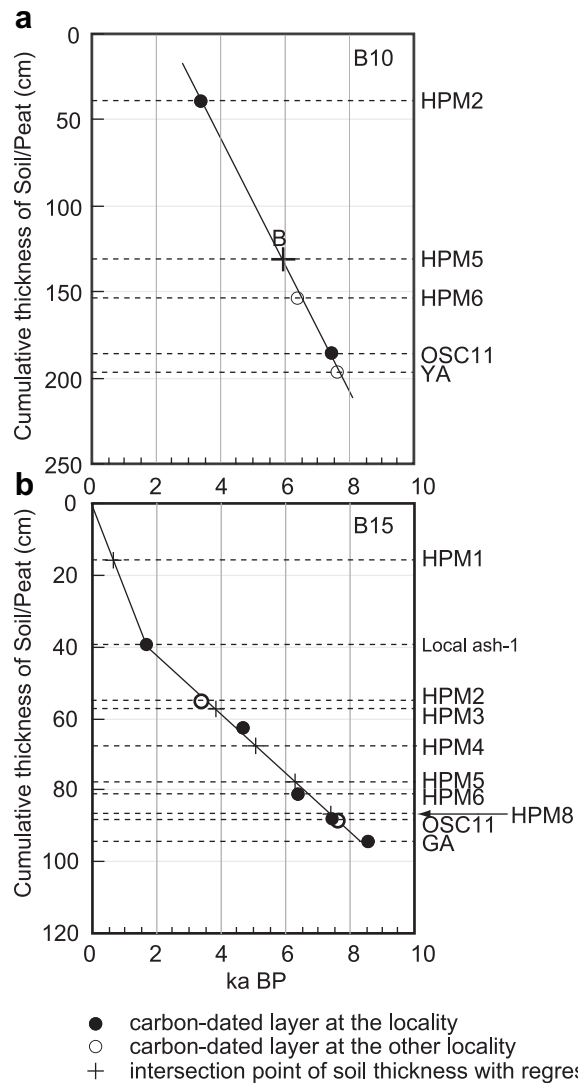


Fig. 14. Relationships between age and cumulative thickness of soil/peat at Sections B10 (a) and B15 (b). Solid circles are dating samples at the section. Open circles indicate dating samples from other correlative sections. Regression lines are drawn by the solid and open circles. Crosses show estimated ages based on the intersection of the regression lines and actual soil thickness.

these estimated values are uncertain, they indicate the order of eruptive volume (that is VEI > 3) of each tephra layer.

7.3. Holocene eruptive history

The age of the lowermost eruptive unit, PPM3, is estimated to be around 10,000 BP because the directly overlying peat layer indicates a date of $9900 \pm 50 \text{ BP}$. This implies that the pyroclastic eruptions from the CTL volcanic chain and Fuss described by our research all belong to the Holocene. New radiocarbon data and estimated age from the soil thickness determined the possible age of each explosive eruption and the Lomonosov lava flow as shown in Fig. 17. The Holocene activity in this region was initiated by PPM eruptions from Tatarinov (or Lomonosov), followed by the effusion of Lomonosov lava after the subordinate lahar and debris avalanche depositions. After the Tatarinov and Lomonosov eruptions, the eruptive center of the CTL volcanic chain shifted to the north, and two volcanoes, Chikurachki and Fuss, started their explosive activity. During the last 7500 years, more than 30 explosive

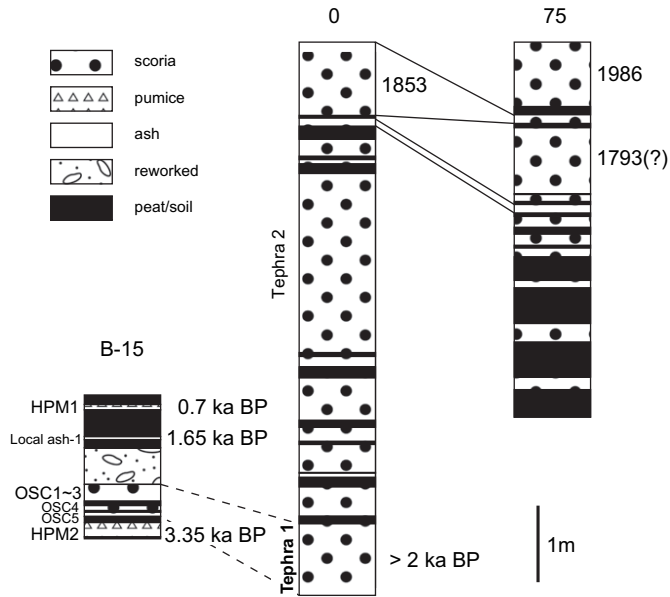


Fig. 15. Examples of stratigraphic columns between the western and eastern side of the Chikurachki volcano. B-15 is a simplified column of that of Fig. 5. Sections 0 and 75 are those of Belousov et al. (2003). The location of Section 0 is shown in Fig. 3. Section 75 is located 4 km northeast of Section 0. The total thickness of soil/peat layer at Section 0 is approximately 1 m. If soil accumulation rate is overestimated as 50 cm/ky, the age of the lowermost “Tephra1” could be estimated to be at least 2 ka BP.

eruptions of both Fuss and Chikurachki have been recorded without long dormancies for more than one thousand years (Belousov et al., 2003 and this study). Eight layers (HPM ones) of those were derived from Fuss, whereas all of the other layers are from Chikurachki. The Fuss summit may have been filled by a crater lake prior to the HPM4 and HPM1 eruptions, resulting in phreatoplinian deposits.

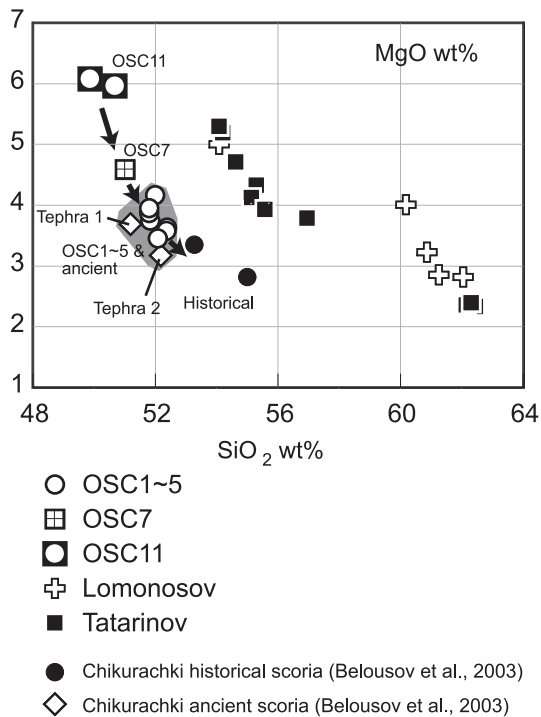


Fig. 16. The MgO–SiO₂ variation diagram for whole-rock chemistry of the Chikurachki group. Arrows indicate a temporal variation of compositions of Chikurachki scoria.

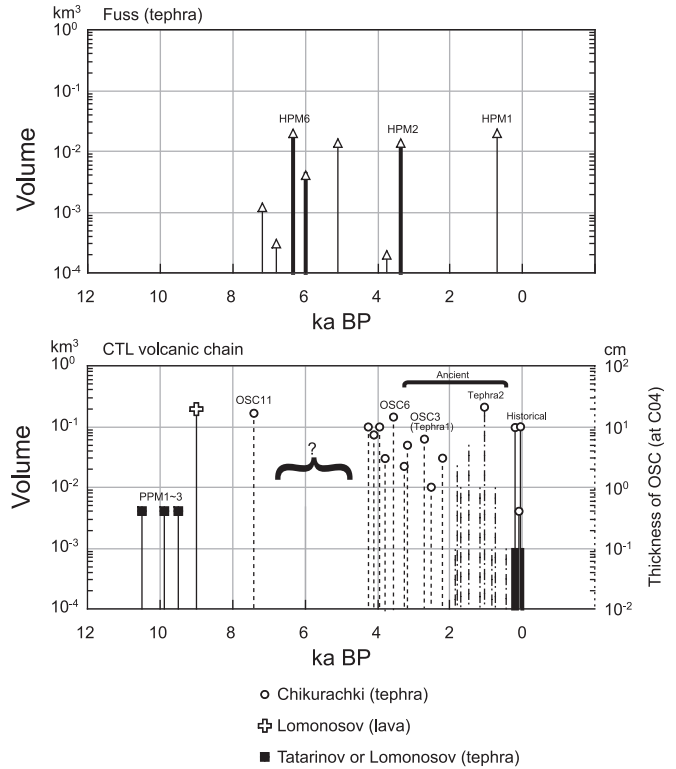


Fig. 17. Volumes and ages of major eruptions from the Fuss (upper) and the Chikurachki group (lower). Volumes of Chikurachki historical eruptions are referenced from Belousov et al. (2003). Dashed bars are the rough estimation volumes based on the geological information of Belousov et al. (2003) and this study (see text for detail). The volumes of PPM2 and 3 were temporarily determined as large as overlying pyroclastic flow deposit (PPM1). 10⁻³–10⁻² km³: VEI = 2, 10⁻²–10⁻¹ km³: VEI = 3, 10⁻¹–1 km³: VEI = 4.

The volume of each explosive Fuss eruption was less than 0.02 km³ (Fig. 17). This suggests that the fieldwork at the eastern flank of Fuss could cover almost all of its explosive eruptions larger than VEI = 2 because this area is located on the leeward side of the volcano. In contrast, all the explosive Chikurachki eruptions ranged from VEI > 3 (Fig. 17), but many of the explosive Chikurachki eruptions with the relatively smaller scale (VEI = 2) could not be identified. Considering a number of missing eruptions of Chikurachki after 2 ka BP in this studied area, Chikurachki has repeated explosive eruptions more frequently than Fuss. In addition, some of these Chikurachki eruptions were relatively large (VEI = 3). In conclusion, after the effusion of the Lomonosov lava (after 9 ka BP), the magma discharge rate of Chikurachki was much higher during the Holocene in comparison to other volcanic centers in this area, a feature consistent with Chikurachki being the highest edifice in this region at present.

7.4. Temporal evolution of magma system

The Kurile arc extending from the Kamchatka–Kurile Islands to Hokkaido is considered to be a typical arc–trench system, in which volcanic rocks show obvious across-arc compositional variations (Popolitov and Volynets, 1982; Avdeiko et al., 1991; Ishikawa and Tera, 1997; Bindeman and Bailey, 1999; Nakagawa, 1999; Nakagawa et al., 2002). Volcanic rocks from the CTL volcanic chain show medium–K compositions, whereas those from Fuss are high–K (Fig. 9). This is consistent with the location of these volcanoes: the CTL chain and Fuss are located at the frontal and back-arc sides of the northern Kurile Islands, respectively (Fig. 1). The same

relationship is also recognized in the case of other incompatible elements, such as Rb and Ba (Fig. 10). Although both the Chikurachki (CTL volcanic chain) and Fuss volcanoes have simultaneously continued eruptive activity, each magma system of the two volcanoes was distinct and has been independently constructed.

The eruptive rocks of Chikurachki are basalt and basaltic andesite. Their SiO₂ and MgO contents gradually increase and decrease with time, respectively (Fig. 16), whereas their K₂O contents increase with increasing SiO₂ content to form a single trend (Fig. 13). During the 7500 years since the OSC11 eruption, no obvious evidence has suggested the input of different magmas into the pre-existed magma system beneath the volcano because whole-rock and matrix glass K₂O contents have not largely changed, in accordance with the SiO₂ content (Figs. 9 and 11). These trends strongly suggest that the magma system composed of basaltic magma was voluminous, and changed its chemistry due to fractional crystallization.

On the other hand, gray and banded pumice were found in almost all the tephra layers of Fuss, indicating that the injection of mafic magma into the felsic system had occurred during each eruption. Thus, the Fuss magma plumbing system was composed of two types of magma: mafic and felsic. The compositional fields of glass chemistries for Fuss pumices are distinct between each eruption unit on the K₂O–SiO₂ diagram and can be divided into five clusters that show different K₂O levels at the similar SiO₂ contents (Fig. 12). These indicate that the felsic magma system of the volcano was short lived and has been replaced by distinct, small felsic magma batches before almost all major eruptions.

On the other hand, the gray pumices show similar K₂O levels (K₂O = 3.5–4.5 wt.%) among the eruptions at SiO₂ = 65–70 wt.%. This suggests that the mafic magma could not be a parental magma that produced all of the felsic magmas with variable K₂O contents, ranging from 3.7 to 6.2 wt.% at SiO₂ = 69–77 wt.%. Thus, the felsic magma batches beneath Fuss were produced either by fractional crystallization of distinct parental mafic magma or the melting of different crustal materials. To discuss the origin of the magma system beneath the volcano, more geochemical data, such as isotope ratios, would be needed.

The frequent replacement of the magma batch under a polygenetic composite volcano such as Fuss has been reported in other volcanoes (Nakagawa et al., 1999; Hobden et al., 1999, 2002). In the case of Chikurachki, however, frequent changes in the magma system have not been observed during the last 7500 years. This is due to the large scale of the magma system beneath the volcano, which was composed of voluminous basaltic magma. Even if a smaller magma batch of other basaltic magma had been injected into the system, it would be hard to detect the chemical shift of eruptive materials. The magma production system of the Chikurachki volcano could produce a similar basaltic magma continuously supplied to the pre-existing system. In Fuss, by contrast, the magma injected into the shallower magma system was recognized by evidence of magma mixing because the shallower system has been small.

Both the Chikurachki and Fuss volcanoes were active under the same subduction system, but the volcano with the higher magma discharge rate, Chikurachki, would continue eruptive activity under a large, stable magma system, whereas the volcano characterized by a lower magma discharge rate, Fuss, could be constructed by an intermittent supply of distinct, small magma batches.

7.5. Evaluation of Holocene eruptive activity of the Chikurachki and Fuss volcanoes

According to the temporal and spatial shift of eruption centers and the scale of eruption (Fig. 17), active periods of explosive

eruptions have alternated between Fuss and Chikurachki. Although this study could not detect any explosive eruptions of the Chikurachki volcano from 7 to 5 ka BP, Fuss had repeated explosive eruptions during this period. The Chikurachki volcano may have changed its mode of eruption to be effusive during this period. Since approximately 4 ka BP, the activity of Chikurachki has increased to a considerable scale of repeated explosive eruption, although the explosive activity of Fuss has decreased. This also suggests that Fuss changed its mode of eruption to effusive. From 2 ka BP to several hundred years ago, no remarkable tephra layers from the Chikurachki volcano occurred in this studied area, but scoria fall deposits on the same horizon have been recognized on the eastern flank of the volcano (Fig. 15), indicating that the scale of each eruption or the magma discharge rate decreased during this time. A relatively larger plinian eruption occurred at Fuss during this period (HPM1). During the last 200 years, Chikurachki had frequent repeated explosive eruptions and was one of the most active volcanoes in the Kurile arc. Only one small eruption has been recorded in Fuss during the last 200 or 300 years (Gorshkov, 1970).

The harmonic change of eruptive activity described above, including the temporal change in either eruption frequency or mode, explosive or effusive, suggests that the magma plumbing and transport systems reaching the surface affect each other. However, as mentioned before, the magma systems of both volcanoes have been isolated and were derived from a distinct source. A similar case is reported in eastern Hokkaido, the southern end of the Kurile arc (Hasegawa et al., 2009). In this region, two volcanoes located 10 km apart, Mashu and Atosanupuri, have continued eruptive activity for over 35,000 years. During this period, however, one volcano repeated explosive eruptions, whereas the other effused lavas. In the southern Paramushir Island and eastern Hokkaido cases, the harmonic eruptive activity of the neighboring two volcanoes may be affected not by the relationship of magma generation and storage systems but by change of the local stress field of the volcanic region. If one of the volcanoes in the region started eruptions, magma discharge through the crust could reflect the local stress field.

8. Conclusions

The tephrostratigraphical, tephrochronological and petrological analyses of four volcanoes on the southern part of Paramushir Island are summarized, as follows:

1. More than 40 tephra units have been described, all of which are separated by paleosols or peat layers. Twenty-seven of these units were distributed widely in the studied area, and each layer was correlated by petrography and whole-rock and glass chemistry.
2. In addition to the units mentioned above, two widespread ash layers, dated at 8.5 ka and 7.6 ka BP, were found in this region. The upper ash was derived from the Kurile Lake caldera on the Kamchatka peninsula.
3. The rocks from the CTL volcanic chain, including Chikurachki, are medium-K, and those from Fuss are high-K. The whole-rock chemical compositions of the rocks of the CTL chain were also distinguished among each center, suggesting a distinct magma system for each. These petrological differences enable determination of the source volcano of each tephra unit.
4. Eruptions of the Tatarinov and Lomonosov volcanoes in the south of the CTL volcanic chain initiated the Holocene eruptive activity in this region. After these activities, Chikurachki and Fuss started their explosive activity at ca. 7.5 ka BP. Of the two volcanoes, Chikurachki has erupted more frequently with a higher magma discharge rate.

5. Considering the temporal variations of juvenile materials during the last 7500 years, Chikurachki has continued eruptive activity with a stable, large magma system, in which the basaltic magma has changed its chemistry primarily by fractional crystallization. On the other hand, beneath Fuss, distinct small magma batches have frequently replaced a smaller magma system.
6. A harmonic change in the frequency and mode of eruption might exist between the Chikurachki and Fuss volcanoes, likely affected by changes in the local stress field caused by the eruptive activity of each volcano.

Acknowledgments

We thank L. Kotenko, S. Marshuk, N. Kolotilin and A. Timofeeva for their fieldwork assistance. We also appreciate A. Matsumoto, H. Nomura and K. Nakamura, for the XRF and SEM-EDS analysis and making the thin sections. Thanks are also due to the editor T. Suzuki, C. van den Bogaard and two anonymous reviewers. This study was financially supported by JSPS funding (nos. 17253002 and 22253005) to MN.

References

- Avdeiko, G.A., Volynets, O.N., Antonov, A.Tu., Tsvetkov, A.A., 1991. Kurile island-arc volcanism: structural and petrological aspects. *Tectonophysics* 199, 271–287.
- Bailey, J.C., Frolova, T.I., Burikova, I.A., 1989. Mineralogy, geochemistry and petrogenesis of Kurile island-arc basalts. *Contributions to Mineralogy and Petrology* 102, 265–280.
- Belousov, A.B., Belousova, M.G., Grushin, S.Yu., Krestov, P.B., 2003. Historic eruptions of the Chikurachki volcano (Paramushir, Kurile Islands). *Volcanology and Seismology* 2003 (3), 15–34 (in Russian with English abstract).
- Bice, D.C., 1985. Quaternary volcanic stratigraphy of Managua, Nicaragua: correlation and source assignment for multiple overlapping plinian deposits. *Geological Society of America Bulletin* 96, 553–566.
- Bindeman, I.N., Bailey, J.C., 1999. Trace elements in anorthite megacrysts from the Kurile island arc: a window to across-arc geochemical variations in magma compositions. *Earth and Planetary Sciences Letters* 169, 209–226.
- Braitseva, O.A., Melekestev, I.V., Ponomareva, V.V., Sulerzhitsky, L.D., 1995. Ages of calderas, large explosive craters and active volcanoes in the Kuril-Kamchatka region, Russia. *Bulletin of Volcanology* 57, 383–402.
- Cao, L.-Q., Arculus, R.J., McKelvey, B.C., 1995. Geochemistry and petrology of volcanic ashes recovered from sites 881 through 884: a temporal record of Kamchatka and Kurile volcanism. *Proceedings of the Ocean Drilling Program, Scientific Results* 145, 345–381.
- Clark, S.K., Reagan, M.K., Trimble, D.A., 2006. Tephra deposits for the past 2600 years from Irazu Volcano, Costa Rica. *Geological Society of America, Special Paper* 412, 225–234.
- Fierstein, J., Nathenson, M., 1992. Another look at the calculation of fallout tephra volumes. *Bulletin of Volcanology* 54, 156–167.
- Gill, J.B., 1981. What is “typical calcalkaline andesite”. In: Gill, J.B. (Ed.), *Orogenic Andesites and Plate Tectonics*. Springer-Verlag, New York, pp. 1–12.
- Girina, O.A., Malik, N.A., Kotenko, L.V., 2008. 2002–2007 activity of Chikurachki volcano (Paramushir island, northern Kuriles) based on KVERT data. *Bulletin of Kamchatka Regional Association* 1 (11), 67–73 (in Russian with English abstract).
- Gorshkov, G.S., 1970. *Volcanism and the Upper Mantle. Investigations in the Kurile Island Arc*. Plenum Press, New York, 385 pp.
- Gurenko, A.A., Belousov, A.B., Trumbull, R.B., Sobolev, A.V., 2005. Explosive basaltic volcanism of the Chikurachki volcano (Kurile arc, Russia): insights on pre-eruptive magmatic conditions and volatile budget revealed from phenocryst-hosted melt inclusions and groundmass glasses. *Journal of Volcanology and Geothermal Research* 147, 203–232.
- Hasegawa, T., Kishimoto, H., Nakagawa, M., Itoh, J., Yamamoto, T., 2009. Eruptive history of post-caldera volcanoes of Kutcharo caldera, eastern Hokkaido, Japan, as inferred from tephrostratigraphy in the Konsen and Shari areas for the period 35–12 ka. *Journal, Geological Society of Japan* 115, 369–390 (in Japanese with English abstract).
- Hobden, B.J., Houghton, B.F., Davidson, J.P., Weaver, S.D., 1999. Small and short-lived magma batches at composite volcanoes: time windows at Tongariro volcano, New Zealand. *Journal, Geological Society of London* 156, 865–868.
- Hobden, B.J., Houghton, B.F., Nairn, I.A., 2002. Growth of a young, frequently active composite cone: Ngauruhoe volcano, New Zealand. *Bulletin of Volcanology* 64, 392–409.
- Ishikawa, T., Tera, F., 1997. Source, composition and distribution of the fluid in the Kurile mantle wedge: constraints from across-arc variations of B/Nb and B isotopes. *Earth and Planetary Sciences Letters* 152, 123–138.
- Kutterolf, S., Freundt, A., Peréz, W., Wehrmann, H., Schmincke, H.-U., 2007. Late Pleistocene to Holocene temporal succession and magnitudes of highly-explosive volcanic eruptions in west-central Nicaragua. *Journal of Volcanology and Geothermal Research* 163, 55–82.
- Legros, F., 2000. Minimum volume of a tephra fallout deposits estimated from a single isopach. *Journal of Volcanology and Geothermal Research* 96, 25–32.
- Miyashiro, A., 1974. Volcanic rock series in island arcs and active continental margins. *American Journal of Science* 274, 321–355.
- Nakagawa, M., 1999. Origin of spatial compositional variations in differentiated arc volcanics at arc-arc junctions: a case study of major and trace element variations in Quaternary volcanics from Hokkaido, Japan. *Resource Geology Special Issue* 20, 159–174.
- Nakagawa, M., Wada, K., Thordarson, T., Wood, C.P., Gamble, J.A., 1999. Petrologic investigations of the 1995 and 1996 eruptions of Ruapehu volcano, New Zealand: formation of discrete and small magma pockets and their intermittent discharge. *Bulletin of Volcanology* 61, 15–31.
- Nakagawa, M., Ishizuka, Y., Kudo, T., Yoshimoto, M., Hirose, W., Ishizaki, Y., Gouchi, N., Katsui, Y., Alexander, S., Steinberg, G.S., Abdurakhmanov, A.I., 2002. Tyatya volcano, southwestern Kuril arc: recent eruptive activity inferred from widespread tephra. *The Island Arc* 11, 236–254.
- Nemoto, T., Sasa, Y., 1960. Geological map sheets of the Kuril Islands (1/250,000 scale).
- Newhall, C.G., Self, S., 1982. The volcanic explosivity index (VEI): an estimate of explosive magnitude for historical volcanism. *Journal of Geophysical Research* 87, 1231–1238.
- Ostapenko, V.F., Fedorchenko, V.I., Shilov, V.N., 1967. Pumices, ignimbrites and rhyolites from the Great Kurile Arc. *Bulletin of Volcanology* 30, 81–92.
- Ovsyannikov, A.A., Muraviev, Y.D., 1992. The 1986 eruption of Chikurachki volcano. *Volcanology and Seismology* 1992 (5, 6), 3–20 (English translation: 1993, 14, 493–514).
- Ponomareva, V.V., Kyle, P.R., Melekestev, I.V., Rinkliff, P.G., Dirksen, O.V., Sulerzhitsky, L.D., Zaretskaia, N.E., Rourke, R., 2004. The 7600 (¹⁴C) year BP Kurile Lake caldera-forming eruption, Kamchatka, Russia: stratigraphy and field relationships. *Journal of Volcanology and Geothermal Research* 136, 199–222.
- Popolitov, E.I., Volynets, O.N., 1982. Geochemistry of Quaternary volcanic rocks from Kurile-Kamchatka island arc. *Journal of Volcanology and Geothermal Research* 12, 299–316.
- Prueher, L.M., Rea, D.K., 2001. Tephrochronology of the Kamchatka-Kurile and Aleutian arcs: evidence for volcanic episodicity. *Journal of Volcanology and Geothermal Research* 106, 67–87.
- Seymour, K.S., Christanis, K., Bouzinos, A., Papazisimou, S., Papatheodorou, G., Moran, E., Denes, G., 2004. Tephrostratigraphy and tephrochronology in the Philippi peat basin, Macedonia, Northern Hellas (Greece). *Quaternary International* 121, 53–65.
- Siebert, L., Simkin, T., 2002. *Volcanoes of the world: an illustrated catalog of Holocene volcanoes and their eruptions*. In: *Global Volcanism Program Digital Information Series, GVP-3*. Smithsonian Institution. <http://www.volcano.si.edu/world/>.
- Smith, R.T., Houghton, B.F., 1995. Delayed deposition of plinian pumice during phreatoplinian volcanism: the 1800-yr-B.P. Taupo eruption, New Zealand. *Journal of Volcanology and Geothermal Research* 64, 221–226.
- Stuiver, M., Reimer, P.J., Reimer, R.W., 2005. CALIB 5.0 [WWW program and documentation]. Available from: <http://calib.qub.ac.uk/calib/>.
- Tamura, Y., Tatsumi, Y., Zhao, D., Kido, Y., Shukuno, H., 2002. Hot fingers in the mantle wedge: new insights into magma genesis in subduction zones. *Earth and Planetary Sciences Letters* 197, 105–116.
- Wentworth, C.K., 1922. A scale of grade and class terms for clastic sediments. *Journal of Geology* 30, 377–392.
- Wulf, S., Kraml, M., Keller, J., 2008. Towards a detailed distal tephrostratigraphy in the Central Mediterranean: the last 20,000 yrs record of Lago Grande di Monticchio. *Journal of Volcanology and Geothermal Research* 177, 118–132.
- Zaretskaia, N.E., Ponomareva, V.V., Sulerzhitsky, L.D., Dirksen, O.V., 2001. Radiocarbon dating of the Kurile Lake caldera eruption (South Kamchatka, Russia). *Geochronometria* 20, 95–102.